Chapter 5

Heterogeneous base catalyst derived from waste *Musa* AAA plant for production of biodiesel

5.1 Introduction

"A potential catalyst from agro-waste can be derived from the banana plant. Banana is one of the most extensively grown-up herbaceous plants in the world, cultivated in over 130 countries for fruit, producing about 16 % of total global production of fruits (Mohapatra et al., 2010). India ranks first among the banana-producing countries, contributing 27 % of global banana production (Mohapatra et al., 2010; Kumar et al., 2013). After the post-harvest of the total cultivated plants, 40 % of the production remains as waste (Pyar and Peh, 2018). The peel, trunk, rhizome, rachis, leaf sheath and peduncle part of the banana plant are the main waste materials. These waste materials have many applications depending on their chemical composition (Balajii and Niju, 2019). Some researchers reported the preparation of catalysts from banana plants and employed these in biodiesel production. Some of these reported catalysts are *Musa acuminata* peduncle (Balajii and Niju, 2019), *Musa* 'Gross Michel' (Betiku et al., 2016), *Musa balbisiana* Colla peel (Gohain et al., 2017), peels of *Musa paradisiacal* (Betiku and Ajala, 2014), peduncle of pisang awak (Balaji and Niju, 2020) and K_2O-KCl based catalyst made from the peel of banana (Fan et al., 2019).

There are many varieties of bananas popularly cultivated in Assam, India. Banana plants have originated in India and the Eastern Asian region (Malaysia and Japan) (Mohapatra et al., 2010). Varieties of bananas have different origins from the same genus *Musa*, and it belongs to the *Musaceae* family. Human-edible bananas are derivatives of the *Australimusa* and *Eumusa* series (Ahmad and Danish, 2018). Most of the edible bananas are a hybrid of the two wild diploid species of *Musa balbisiana* Colla and *Musa acuminata* Colla (Mohapatra et al., 2010). Mainly, banana comprises high concentrations of K along with other metals (Gohain et al., 2017; Atim et al., 2013; Balaji and Niju, 2020). In this study, considering the nature of bananas, the post-harvested banana waste was focused to generate a potential, effective, and cheap catalyst. The primary goal of the current study is to comparatively investigate the activities of the catalysts derived from the rhizome, stem and peel part of Bharatmoni banana found in Assam (India) for the biodiesel preparation from *Jatropha curcas* oil and methanol via the transesterification process. Bharatmoni banana belongs to the AAA genome group

(Borborah et al., 2020). Bharatmoni banana (*Musa* AAA) is widely grown in the northeastern part of India mainly in Assam. Its fruit peel color does not turn completely yellow even if it is ripened. The green color remains on the edges of the fruit even after ripening and it has thick fruit peel. Commonly, its fruit length is around 13.75 cm and its fruit circumference is 10.20 cm. The Bharatmoni banana plant has mostly 6–7 hands per bunch bearing 78–90 fingers on it. As per another study reported by Saikia et al. (2020), the Bharatmoni banana fills fruit within the lowest duration of 53.5 days than other varieties of banana. This work reported the comparison of activities of the catalysts in biodiesel generation, reaction kinetics, and thermodynamics parameters along with chemical composition and reusability of the material catalyst prepared from Bharatmoni peel, stem, and rhizome. The determination of fuel properties of produced biodiesel was also reported (Basumatary et al., 2024). In this work, the post-harvested waste materials from the Bharatmoni banana plant were successfully turned into an effective catalyst that can be applied for the production of biodiesel at commercial scale.

5.2 Experimental

5.2.1 Chemicals and materials

The Bharatmoni banana plant was collected from Kokrajhar, Assam, India in February 2021. *J. curcas* oil was obtained from India Mart and used as a feedstock. The chemicals used in this study were similar as mentioned in Chapter 2 **(Section 2.2.1**, **Page no. 34)**

5.2.2 Preparation of catalysts

After collection, the Bharatmoni banana plant was portioned out into three parts *viz*. stem, peel, and rhizome (**Fig. 5.1**). These three parts were cut again into small slices and dried under sunlight for 14-15 days. Further steps of preparation are same as described in Chapter **2 (Section 2.2.2.1, Page no. 34**). In the present study, altogether six varieties of catalysts, three burnt catalysts and three calcined catalysts derived from the Bharatmoni were explored in transesterification reactions, and these six catalysts were named and abbreviated as Burnt Bharatmoni peel (BBP), Burnt Bharatmoni stem (BBS), Burnt Bharatmoni rhizome (BBR), Calcined Bharatmoni peel at 550 ^{o}C (CBP-550), Calcined Bharatmoni stem at 550 ^{o}C (CBS-550) and Calcined Bharatmoni rhizome at 550 ^{o}C (CBR-550).

Fig. 5.1. Pictorial representation of raw materials of Bharatmoni banana peel (A-C), stem (D-F) and rhizome (G-I) for catalyst preparation.

5.2.3 Catalyst characterization

To explore the characteristics of the catalysts from the banana plant Bharatmoni, same procedure and sophisticated instruments such as XPS, FT-IR, HRTEM, BET, FE-SEM and EDX were employed as detailed in Chapter **2 (Section 2.2.2.2, Page no. 35-36**). The powder XRD examination was performed by the same instrument as mentioned in Chapter **3 (Section 3.2.2.2, Page no. 91**). Similarly, the pH value, soluble alkalinity and basicity were determined

for calcined catalysts (CBP-550, CBS-550 and CBR-550) which were carried out as per the prescribed protocol mentioned in Chapter **2 (Section 2.2.2.2, Page no. 36**).

5.2.4 Transesterification reaction for the biodiesel synthesis

In this chapter, the transesterification reactions were loaded with the prepared catalysts (CBP-550, CBS-550, and CBR-550) varying their wt. % with respect to oil. The protocol of experiments for the synthesis of biodiesel via transesterification, analysis of optimum reaction conditions (ORCs) and the calculation of biodiesel yield % were carried out with the same procedure as described in **Chapter 2 (Section 2.2.2.3, Page no. 36-37**).

5.2.5 Analysis of produced biodiesel

The characterization of obtained biodiesel and *J. curcas* oil were analyzed by FT-IR, ^{1}H NMR and GCMS with the similar protocol described in **Chapter 3 (Section 3.2.2.3, Page no. 92**). The physicochemical analyses of the produced biodiesel were determined by following same protocol and equation as mentioned in **Chapter 2 (Section 2.2.2.3, Page no. 37-38**). The acid value (AV) of oil and biodiesel were also obtained by using the same procedure described in **Chapter 3 (Section 3.2.2.3, Page no. 92**).

5.3 Results and Discussion

5.3.1 Characterization of Bharatmoni catalysts

5.3.1.1 Powder XRD analyses of catalysts

The XRD patterns (**Fig. 5.2**) of CBP-550, CBS-550 and CBR-550 catalysts showed the existence of qualitative crystalline materials. In the probed data from XRD patterns, 2θ values were compared in accordance with JCPDS (ICDD 2003) and other reported data in published literature. In the X-ray diffraction pattern of CBP-550, the peaks at 2θ values of 28.41, 40.54, 50.18, 58.72, 66.44 and 73.88 showed the existence of KCl. The peaks obtained at 2θ values of 26.76, 29.79, 30.89, 31.99 and 34.75 referred to the presence of K_2CO_3 in CBP-550. The occurrence of K_2O in CBP-550 was affirmed from the characteristic peak at 2θ = 39.43. The peaks at 2θ values of 25.74, 28.50 and 38.61 represented the existence of SiO_2 in CBP-550. The peaks obtained at 2θ = 32.82, 30.62 and 44.95 corresponds to the existence of CaO, SrO and $CaMg(CO_3)_2$ respectively in the CBP-550 catalyst. Therefore, from the XRD patterns of the CBP-550 catalyst, the components in the catalysts are revealed to be KCl, K_2CO_3, K_2O, SiO_2, CaO, SrO and $CaMg(CO_3)_2$. The sharp peaks with high intensities were identified at 2θ values of 28.27, 40.46, 50.32, 58.59, 66.30 and 73.95 which attribute to KCl component present

in the CBS-550 catalyst. The presence of K_2CO_3 in CBS-550 was detected by the peaks at 2θ = 29.65, 29.93, 31.31 and 31.86. The existence of K_2O was identified from 2θ values of 39.25 and the peaks at 2θ = 32.13, 32.68 and 43.15 clearly denoted the occurrence of CaO in CBS-550. The existence of SiO_2 in the CBS-550 catalyst was described by a diffraction pattern (**Fig. 5.2**) at 2θ values of 25.63 and 28.55. $CaMg(CO_3)_2$ is also existed in the CBS-550 catalyst which was revealed by the characteristic peak at 2θ = 45.36. Except for SrO, the same components also existed in CBS-550 compared with the CBP-550 catalyst. Similarly, the catalyst CBR-550 has a KCl component which is revealed by the peaks at 2θ = 28.21, 40.50, 50.25, 58.74, 66.30 and 73.98. The occurrence of K_2CO_3 in CBR-550 was interpreted from the 2θ values at 26.55, 29.58, 30.14 and 32.06. The K_2O in CBR-550 was characterized by the peaks at 2θ = 39.30 and 48.60. The existence of CaO in CBR-550 was also established from the peaks at 2θ = 32.61 and 43.06. The characterized peaks at 2θ = 25.73 and 28.48 are due to SiO_2, at 2θ = 33.72 due to $CaCO_3$ and at 2θ = 45.34 due to $CaMg(CO_3)_2$ present in CBR-550 catalyst. Hence, the XRD analysis results explained that the CBP-550, CBS-550 and CBR-550 catalysts are mainly composed of carbonates and oxides of K, Ca, Si and Mg which are significantly exhibiting high basicity. The obtained XRD results of the present work are well comparable with XRD data reported in other agro-waste materials *viz*. Poovan banana pseudostem (Niju et al., 2021), *M. acuminata* peel (Daimary et al., 2022a), *M. balbisiana* Colla peel (Gohain et al., 2017), *Carica papaya* peel (Oladipo et al., 2020), waste passion fruit peel (Tarigan et al., 2022), potato peel (Daimary et al., 2022b), and waste *Mangifera indica* peel (Laskar et al., 2020).

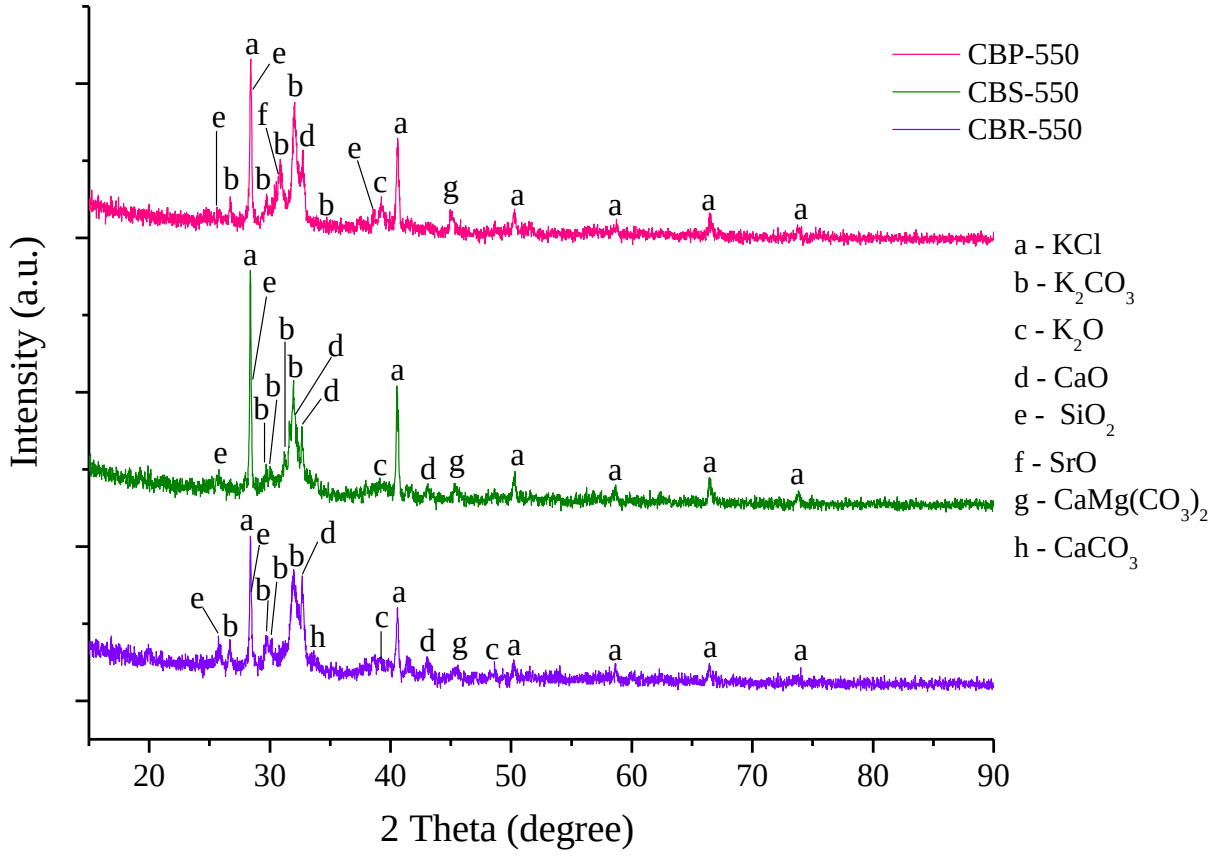

Fig. 5.2. XRD patterns of calcined Bharatmoni catalysts.

5.3.1.2 FT-IR analyses

The FT-IR analyses were conducted for CBP-550, CBS-550, CBR-550 and the 3rd recycled catalysts and the spectra were shown in **Fig. 5.3**. The bands that appeared at the wavenumber of 3482 cm^{-1}, 3485 cm^{-1}, 3478 cm^{-1} and 3437 cm^{-1} are assigned to stretching vibration of the -OH group in the CBP-550, CBS-550, CBR-550 and 3rd recycled catalysts respectively. These indicate the adsorption of water molecules on catalyst's surface (Pathak et al., 2018). The spectra exhibited for the catalyst CBP-550 at 1648 and 1408 cm^{-1}, CBS-550 (1641, 1463, 1401 cm^{-1}), 3rd recycled catalyst (1641, 1470, 1415 cm^{-1}) and for CBR-550 at 1641, 1470, 1401 cm^{-1} are representing the C-O stretching and bending vibrations that refer to the occurrence of carbonate (CO_3^{2-}) (Betiku et al., 2016; Laskar et al., 2020). The metal carbonate present in the catalyst also agreed with the XRD result (**Fig. 5.2**). The peaks located at 1099, 997 and 866 cm^{-1} (CBP-550), 1031 and 866 cm^{-1} (CBS-550), 1024 and 866 cm^{-1} (recovered catalyst of CBS-550) and 1106 cm^{-1} (CBR-550) are due to Si-O-Si bond vibration (Laskar et al., 2020; John et al., 2020). The bands at 757, 660 and 572 cm^{-1} (CBP-550), 702 cm^{-1} (CBS-550), 708 and 613 cm^{-1} (recovered catalyst) and 708 cm^{-1} (CBR-550) are indicative of Ca-O and K-O stretching

bond vibrations (Gohain et al., 2017; Pathak et al., 2018; Falowo et al., 2020). Thus, this FT-IR study is supported by the results found in the XRD analyses (**Fig. 5.2**).

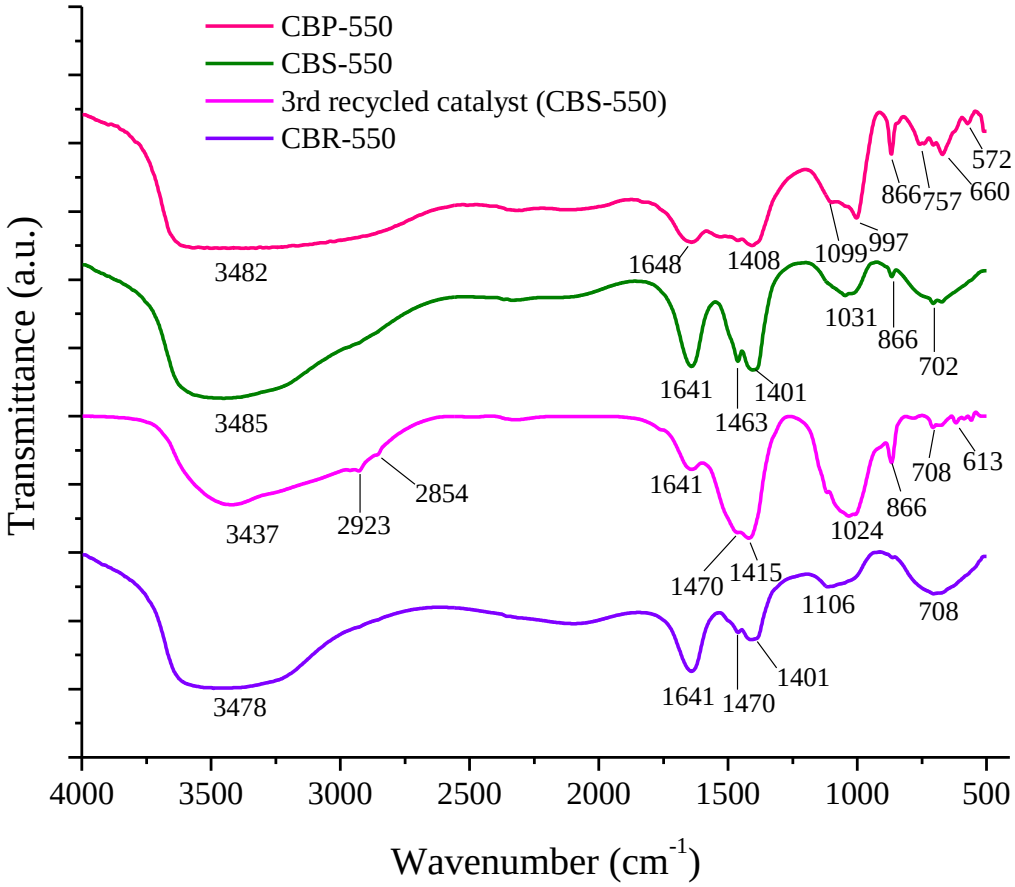

Fig. 5.3. FT-IR spectra of calcined Bharatmoni catalysts.

5.3.1.3 BET study

The BET surface areas of CBP-550, CBS-550 and CBR-550 catalysts were measured as 2.061, 0.730 and 0.857 $m^2 g^{-1}$. The measured pore volumes were 0.008, 0.002 and 0.002 $cm^3 g^{-1}$ for CBP-550, CBS-550 and CBR-550 respectively. Comparable surface areas were also reported in the catalysts prepared from some other biomasses such as peels of tucumã (1.0 $m^2 g^{-1}$) (Mendonça et al., 2019b), straw slag (1.2 $m^2 g^{-1}$) (Wang et al., 2017b) and activated wood ash (0.65 $m^2 g^{-1}$) (Sharma et al., 2012). The method of preparation also influences the surface area, pore volume and pore diameter of the catalyst. Daimary et al. (2022a) reported the change in surface area, pore diameter and pore volume values for the same catalyst (*Musa acuminata* peel) when prepared by two different methods. At high calcination temperatures, catalyst particles agglomerate leading to a low surface area (Miladinovic et al., 2020). According to the isotherm (**Fig. 5.4**), the present catalysts showed type IV physisorption isotherms and

demonstrated an H3 hysteresis loop. In this study, the obtained pore diameter of CBP-550, CBS-550 and CBR-550 catalysts were 4.059, 3.459 and 2.976 nm respectively. The distribution of BJH pore-size of CBP-550, CBS-550 and CBR-550 catalysts are found between the nanoparticle sizes of 2–50 nm confirming that the catalysts are mesoporous in nature. Eldiehy et al. (2020) reported that waste sweet potato leaf-derived catalyst has a mesoporous structure illustrating physisorption isotherm type IV and H3 hysteresis loop. Similar results were reported by Oladipo et al. (2020), Falowo and Betiku (2022) and Betiku et al. (2019), for the catalysts derived from the *Carica papaya* peel, agrowastes mixture and kola nut husk respectively. Although the present catalysts contained low surface areas, they have high catalytic activity which may be due to their porosity character and constituents of basic elements.

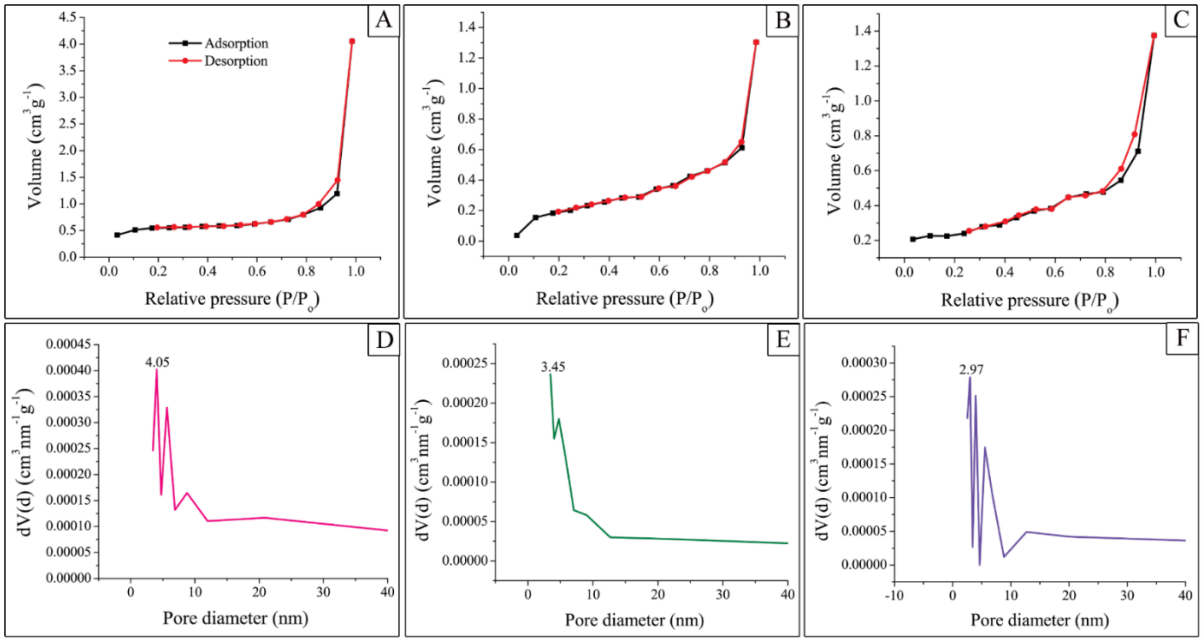

Fig. 5.4. N_2 adsorption-desorption isotherms (A–C) and adsorption pore size distribution of CBP-550 (D), CBS-550 (E) and CBR-550 (F) catalysts.

5.3.1.4 FESEM and HR-TEM analyses

The images analyzed by the FESEM technique are shown in **Fig. 5.5** (burnt ash material), **Fig. 5.6** (calcined catalysts) and **Fig. 5.7** (3rd recycled CBS-550 catalyst). It can be observed that the BBP catalyst exhibited a beads-like shape with holes indicating porosity features (**Fig. 5.5** A). The BBS catalyst has substances aggregated with mostly oval, polygons, and cylindrical shapes along with pores (**Fig. 5.5** C). The analysis also demonstrated the porous nature of the BBR catalyst with compacted rough and aggregated particles (**Fig. 5.5** E). The morphological

difference in FESEM images can be observed in calcined catalysts (**Fig. 5.6**) compared with burnt ash materials (**Fig. 5.5**). The catalyst CBP-550 (**Fig. 5.6** A) revealed the presence of more aggregated components with irregular spherical-like shapes having porous morphology. The surface morphological features of CBS-550 (**Fig. 5.6** C) can be observed as rough clusters of tiny spheres and porous nature. The catalyst CBR-550 has no specific geometrical shapes but it is compact material with porous nature (**Fig. 5.6** E). FESEM analysis of the recovered catalyst from the 3rd reaction cycled (**Fig. 5.7**) showed that its outer morphology is shaped like a crushed cylindrical and oval as if some of the particles are washed out.

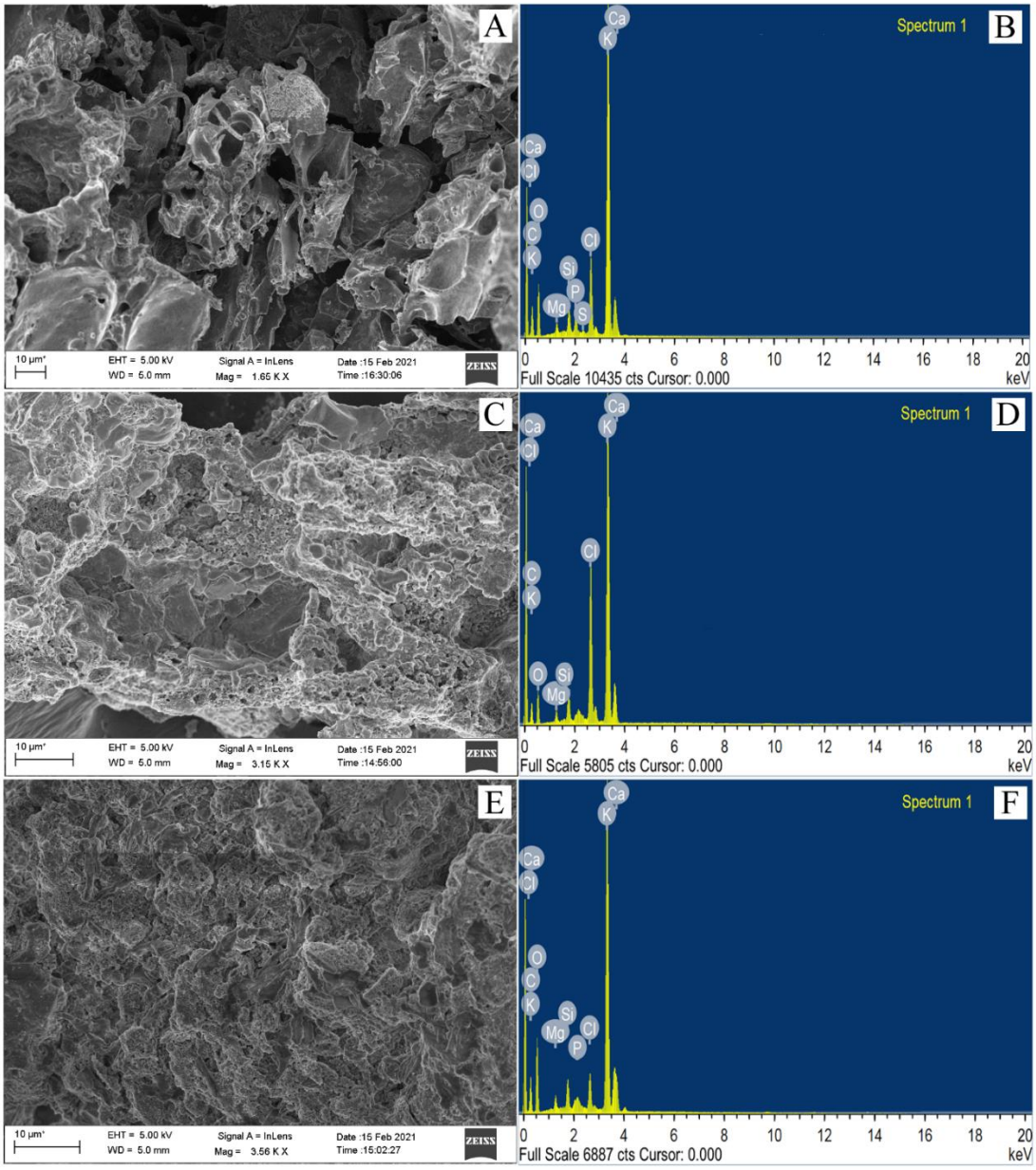

Fig. 5.5. FESEM images (A, C, E) and EDX spectra (B, D, F) of BBP (A, B), BBS (C, D) and BBR (E, F) catalysts.

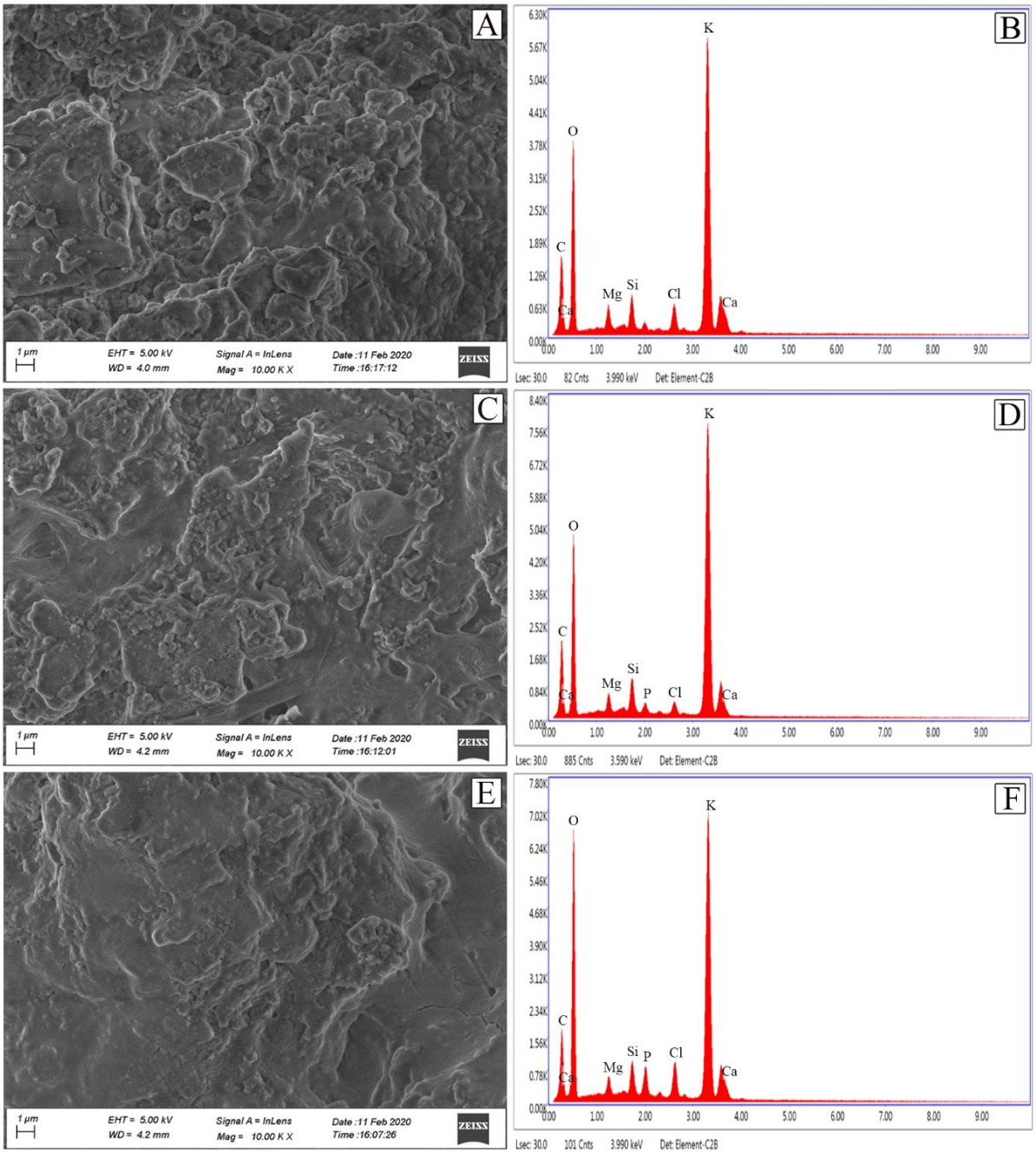

Fig. 5.6. FESEM images (A, C, E) and EDX spectra (B, D, F) of CBP-550 (A, B), CBS-550 (C, D) and CBR-550 (E, F) catalysts.

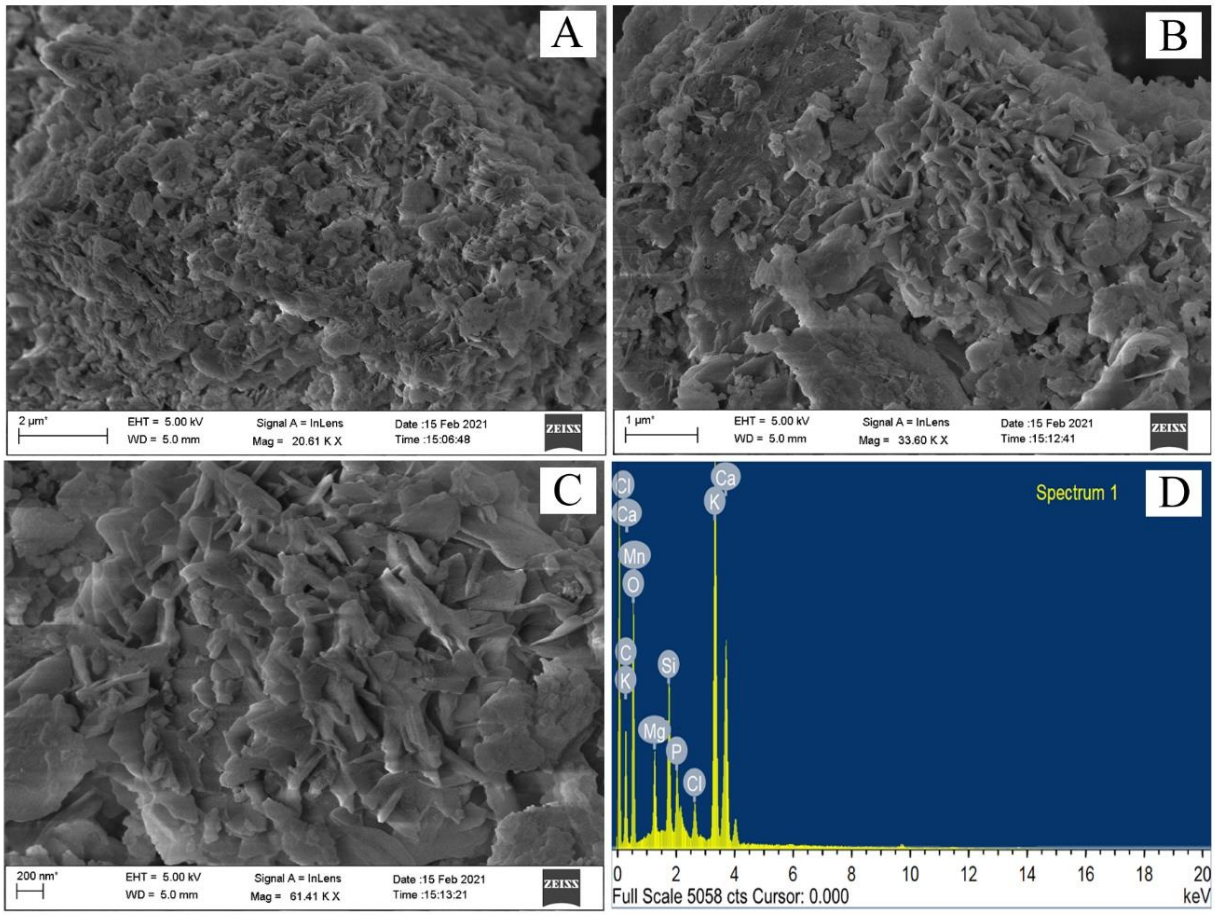

Fig. 5.7. FESEM images (A–C) and EDX spectrum (D) of 3rd recycled catalyst of CBS-550.

The HR-TEM images shown in **Fig. 5.8** (A, B) are for the CBP-550 catalyst which displayed that it has aggregated particles with many non-uniform oval and spherical shapes and looks like porous particles. **Fig. 5.8** (C, D) are the HR-TEM images of the CBS-550 catalyst that also revealed the porous materials and rough surface composed of tiny oval and polygon shapes. Similarly, the surface morphology of the CBR-550 catalyst recorded by the HR-TEM technique as shown in **Fig. 5.8** (E, F) disclosed that the material is built up with compact particles without specific shapes and has some holes indicating its porous property. The existence of porosity of the present calcined catalysts also agreed with the BET study. The morphological results depicted in the FESEM study are supported by the results demonstrated in the HR-TEM studies.

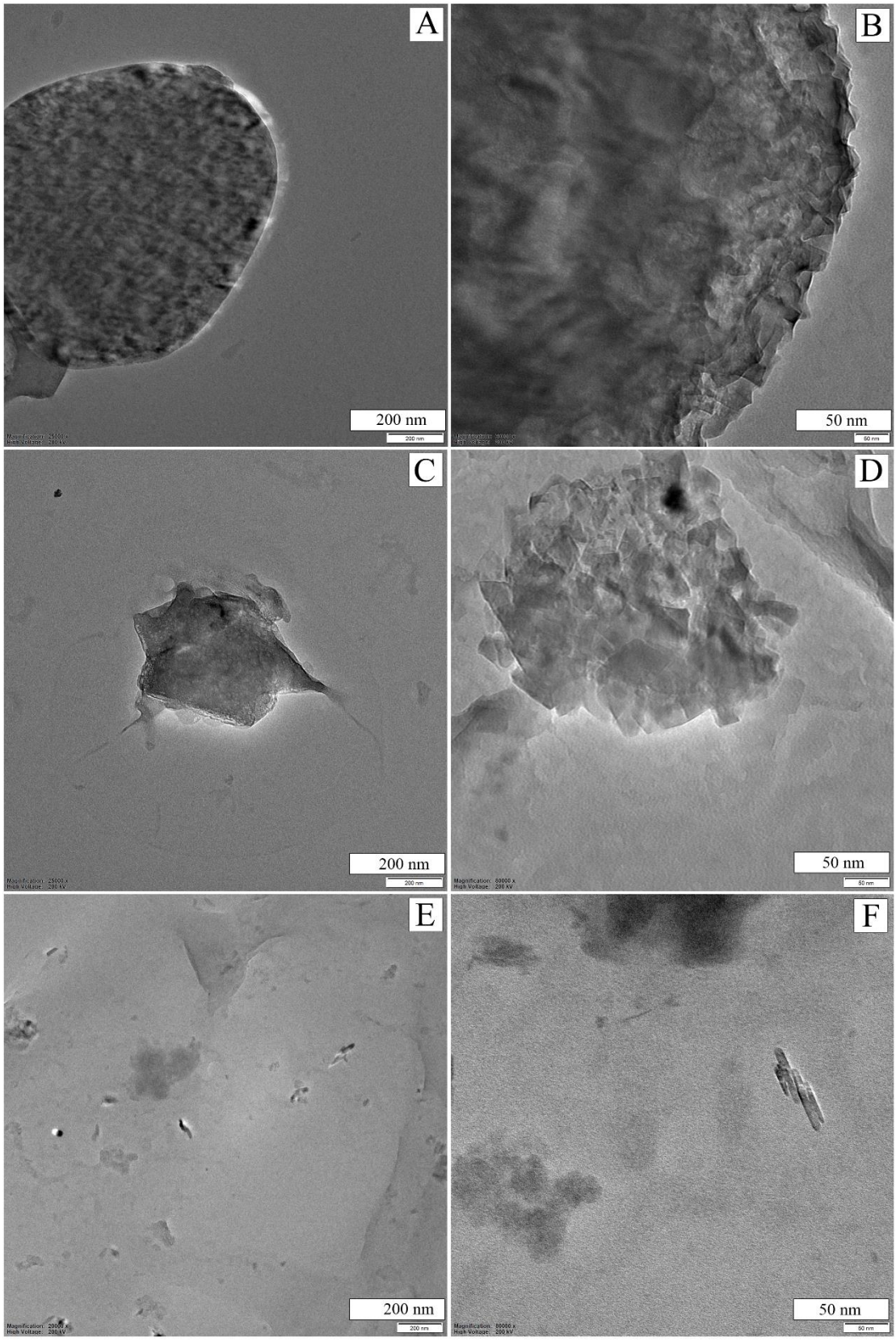

Fig. 5.8. TEM images of CBP-550 (A, B), CBS-550 (C, D) and CBR-550 (E, F) catalysts.

5.3.1.5 EDX analyses of the catalysts

Table 5.1 and **Table 5.2** represent the analyzed elemental compositions of the derived catalysts. The obtained data explains that burnt ash and calcined catalysts of different parts of the Bharatmoni plant exhibit different elemental compositions. **Fig. 5.5** (B, D, F) illustrated the EDX patterns for BBP, BBS and BBR catalysts that indicated the occurrence of K, C, O, Ca, Cl, Mg and Si. Besides these, P is present in BBP and BBR and the S element is also found in BBP catalyst. Among the existing elements, K constituted the highest composition in the BBS (36.53 %) catalyst (**Table 5.1**). The EDX patterns for CBP-550, CBS-550 and CBR-550 are represented in **Fig. 5.6** (B, D, F). After the burnt ash material was calcinated at 550 ^{o}C, it revealed the increase of potassium composition with variable weight % and atomic % (**Table 5.2**). The CBP-550 catalyst consists of 44.88 wt. % of K, CBS-550 catalyst showed 46.88 wt. % of K and CBR-550 catalyst exhibited K of 39.33 wt. %. It is remarkable that among all the catalysts of this study, the CBS-550 catalyst has been observed with the highest quantity of potassium (**Table 5.2**). Since the CBS-550 catalyst has higher K content, it is expected to exhibit more K_2CO_3 and K_2O constituents as depicted in analyses of FT-IR (**Fig. 5.3**) and XRD (**Fig. 5.2**), and that may be a reason for showing the highest catalytic activity. Etim et al. (2021), Gohain et al. (2017) and Tarigan et al. (2022) have also found high K in their catalysts prepared from biomass sources and reported good catalytic activities. In **Table 5.3**, the composition of the elements of the CBS-550 catalyst is compared with other catalysts reported from different biomass sources. From the comparison, it can be understood that the present catalyst (CBS-550) has a higher K concentration showing better catalytic activity than other catalysts mentioned in **Table 5.3**. As the catalyst CBS-550 showed the best activity with high K, it was tested for reusability up to the 3rd cycle and the examined EDX for 3rd recycled catalyst is depicted in **Fig. 5.7** D and its elemental compositions are shown in **Table 5.2**. It is seen that the K concentration in 3rd recycled catalyst has reduced, resulting in reduced catalytic activity due to its decrease in basic site elements. The recycled catalysts of orange peel ash and *Musa champa* peduncle studied by Changmai et al. (2021) and Nath et al. (2023) respectively have also reported the comparable EDX analyzed data with the reduction of active components after being employed in the transesterification reaction.

Table 5.1: FESEM-EDX analyses of burnt Bharatmoni materials.

Elements	Composition of burnt Bharatmoni materials					
	BBP		BBS		BBR	
	Weight %	Atomic %	Weight %	Atomic %	Weight %	Atomic %
C	21.26	34.76	19.68	34.77	17.83	28.73
O	33.83	41.52	25.73	34.12	41.37	50.14
K	32.83	16.48	36.53	19.82	30.80	15.25
Ca	1.16	0.57	1.22	0.60	3.66	1.77
Mg	0.82	0.66	0.91	0.80	1.02	0.82
Si	1.81	1.26	2.15	1.63	1.91	1.32
P	1.70	1.08	-	-	0.48	0.30
Cl	6.42	3.55	13.75	8.22	2.87	1.57
S	0.18	0.11	-	-	-	-

Table 5.2: FESEM-EDX analyses of calcined Bharatmoni catalysts.

Elements	Composition of catalyst calcined at 550 ºC							
	CBP-550		CBS-550		3rd recycled catalyst (CBS-550)		CBR-550	
	Weight %	Atomic %	Weight %	Atomic %	Weight %	Atomic %	Weight %	Atomic %
C	4.67	8.92	6.46	12.15	24.63	35.79	4.55	8.36
O	39.86	57.17	38.96	55.00	45.29	49.41	44.52	61.39
K	44.88	26.34	46.88	27.08	13.06	5.82	39.33	22.19
Ca	3.40	1.95	1.15	0.65	8.18	3.56	2.01	1.11
Mg	1.92	1.81	1.53	1.42	2.29	1.65	1.45	1.32
Si	2.28	1.86	2.49	2.01	3.50	2.17	2.16	1.70
P	-	-	1.00	0.73	1.76	0.99	2.42	1.73
Cl	3.00	1.94	1.52	0.97	1.06	0.52	3.55	2.21
Mn	-	-	-	-	0.19	0.06	-	-

Table 5.3: Elemental composition of Bharatmoni catalyst and its comparison with other reported solid catalysts derived from waste biomasses.

Source of catalyst	Calcination condition	Composition (%)							
		K	**Ca**	**Mg**	**Si**	**P**	**Cl**	**C**	**O**
Bharatmoni stem (This work)	550 ^{o}C, 2 h	46.88	1.15	1.53	2.49	1.00	1.52	6.46	38.96
Passion fruit peel (Tarigan et al., 2022)	400 ^{o}C, 4 h	44.4					16.6	7.9	
Citrus sinensis peel (Changmai et al., 2021)	Burnt	8.95	5.01	1.30	-	-	-	-	37.20
Carica papaya peel (Etim et al., 2021)	700 ^{o}C, 4 h	36.74	3.64	1.16	0.71	4.22	10.3	-	44.1
Musa balbisiana peel (Gohain et al., 2017)	700 ^{o}C, 4 h	41.37	36.08	12.02	–	–	–	–	–
Musa acuminata peduncle (Balajii and Niju, 2019)	Uncalcined	25.63	–	0.97	0.56	0.78	–	–	72.06
Heteropanax fragrans (Basumatary et al., 2021c)	550 ^{o}C, 2 h	19.05	5.13	0.86	8.51	0.64	1.92	16.71	46.74
Camphor leaf (Li et al., 2018)	800 ^{o}C, 2 h	1.22	12.05	1.82	–	–	–	–	–
Musa acuminata peduncle (Balajii and Niju, 2019)	700 ^{o}C, 4 h	42.23	1.70	1.39	1.54	1.91	–	–	50.54
Poovan banana pseudostem (Niju et al., 2021)	700 ^{o}C, 4 h	20.2	7.4	4.52	3.79	1.91	8.99	–	–
Lemna perpusilla (Chouhan and Sarma, 2013)	550 ^{o}C, 2 h	11.32	–	–	82.51	–	–	5.10	–
Pawpaw peel (Oladipo et al., 2020)	600 ^{o}C, 4 h	23.89	2.86	1.00	0.00	3.04	0.87	29.16	36.72
Musa balbisiana underground stem (Sarma et al., 2014)	550 ^{o}C, 2 h	25.09 (K_2O)	10.44 (CaO)	10.04 (MgO)	35.92 (SiO_2)	4.47 (P_2O_5)	–	–	–
Acacia nilotica stem (Sharma et al., 2012)	800 ^{o}C	5.7	17.8	4.5	21.5	0.5	–	–	–
Acacia nilotica stem (Sharma et al., 2012)	500 ^{o}C	6.7	13.3	2.7	15.7	0.80	–	–	–
Moringa leaves (Aleman-Ramirez et al., 2021)	500 ^{o}C, 2 h	9.87	10.09	5.92	–	1.19	–	12.19	59.57
Snail shell (Laskar et al., 2018)	900 ^{o}C, 4 h	-	68.8	0.1	0.3	0.00	-	4.6	26.1
Sesamum indicum (Nath et al., 2020)	550 ^{o}C, 2 h	29.64	33.80	9.68	11.32	–	–	–	–

5.3.1.6 XPS study

XPS analyses results of burnt ash materials (BBP, BBS and BBR), calcined catalysts (CBP-550, CBS-550, CBR-550) and the regenerated catalyst from the 3rd reaction cycle are shown in **Fig. 5.9** and **Fig. 5.10.** The determined surface elemental compositions are summarized in **Table 5.4**. The existence of O, C and K elements are found mainly with high concentration (atomic %) along with Ca, Mg, Fe, Mn, Si, Zn and Sr. The deconvoluted spectrum (**Fig. 5.9** B) of C 1s for BBP was noticed at the binding energies of 284.89 and 288.55 eV. The binding energies observed at 284.86 eV and 288.58 eV for BBS and at 284.81 eV and 288.56 eV for BBR (**Fig. 5.9** B). On the other hand, for calcined catalysts, the presence of C 1s is denoted in **Fig. 5.10** B at two different binding energies of 284.81 and 288.60 eV for CBP-550, 284.70 and 288.32 eV for CBS-550, 284.68 and 288.22 eV for CBR-550 and observed at 284.81 and 284.08 eV for the recovered catalyst. These peaks revealed in XPS spectra for every catalyst signify the occurrence of C=O and C-C bonds that supports the presence of metal carbonates (Changmai et al., 2020a). The XPS spectra for O 1s (**Fig. 5.9** C and **Fig. 5.10** C) revealed binding energies of 530.82eV (BBP), 530.75 eV (BBS), 530.98 eV (BBR), 530.71 eV (CBP-550), 530.60 eV (CBS-550), 530.56 eV (CBR-550) and 531.37 eV (recovered catalyst), indicating the presence of oxygen occurring as metal oxides and carbonates (Eldiehy et al., 2020). **Fig. 5.9** D and **Fig. 5.10** D illustrated two peaks for K 2p at the binding energies of 292.66 and 295.31 eV (BBP), 292.37 and 295.18 eV (BBS), 292.57 and 295.35 eV (BBR), 292.69 eV and 295.32 eV (CBP-550), 292.49 and 295.24 eV (CBS-550), 292.48 and 295.22 eV (CBR-550) and 292.78 and 295.54 eV (3rd recycled catalyst). Out of the appeared two distinct peaks for each catalyst, the lower binding energy ascribed to K $2p_{3/2}$ and the peak at higher binding energy correspond to K $2p_{1/2}$ which demonstrated the existence of K as +1 state in the form of K_2O and K_2CO_3 in all the catalysts of this work (Nath et al., 2023). The two hump peaks appeared (**Fig. 5.9** E and **Fig. 5.10** E) for Ca 2p with the binding energies of 346.63 and 350.18 eV (BBP), 346.65 and 350.14 eV (BBS), 346.67 and 350.30 eV (BBR), 346.58 and 350.17 eV (CBP-550), 346.49 and 350.30 eV (CBR-550) and 346.77 and 350.32 eV (recovered catalyst) established the occurrence of Ca oxide or carbonate in the present catalysts (Brahma et al., 2023). The Si 2p spectra (**Fig. 5.9** F and **Fig. 5.10** F) revealed a single peak at a lower binding energy of 101.88 eV (BBP), 102.42 eV (BBS), 101.79 eV (BBR), 101.83 eV (CBP-550), 101.71 eV (CBS-550), 101.67 eV (CBR-550) and 102.47 eV for the recovered catalyst, and this is due to Si-O bond (Tamuli et al., 2020). The XPS studies of the present catalysts concluded that the calcined catalysts exhibited more concentrations of O, C and K (**Table 5.4**) compared to the burnt ash materials. The

investigated XPS data showed the occurrence of K as one of the dominant elements existing as K_2O and K_2CO_3 in the calcined catalysts, which is mainly responsible for the base catalysis of this study. These data also coincided with the results of the EDX (**Table 5.2**) investigations.

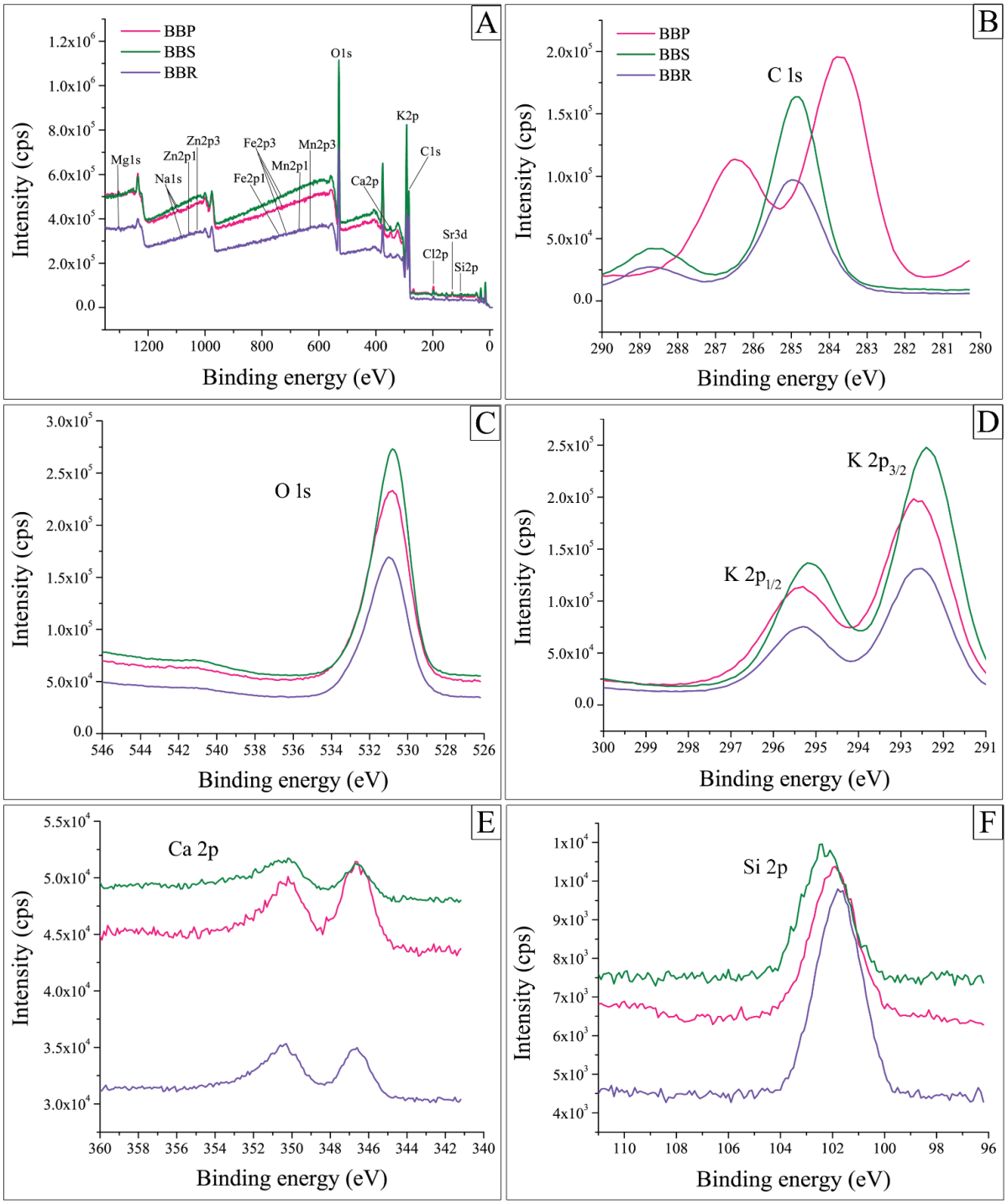

Fig. 5.9. XPS survey spectra (A) of BBP, BBS, BBR catalysts; XPS patterns of C 1s (B), O 1s (C), K 2p (D), Ca 2p (E) and Si 2p (F).

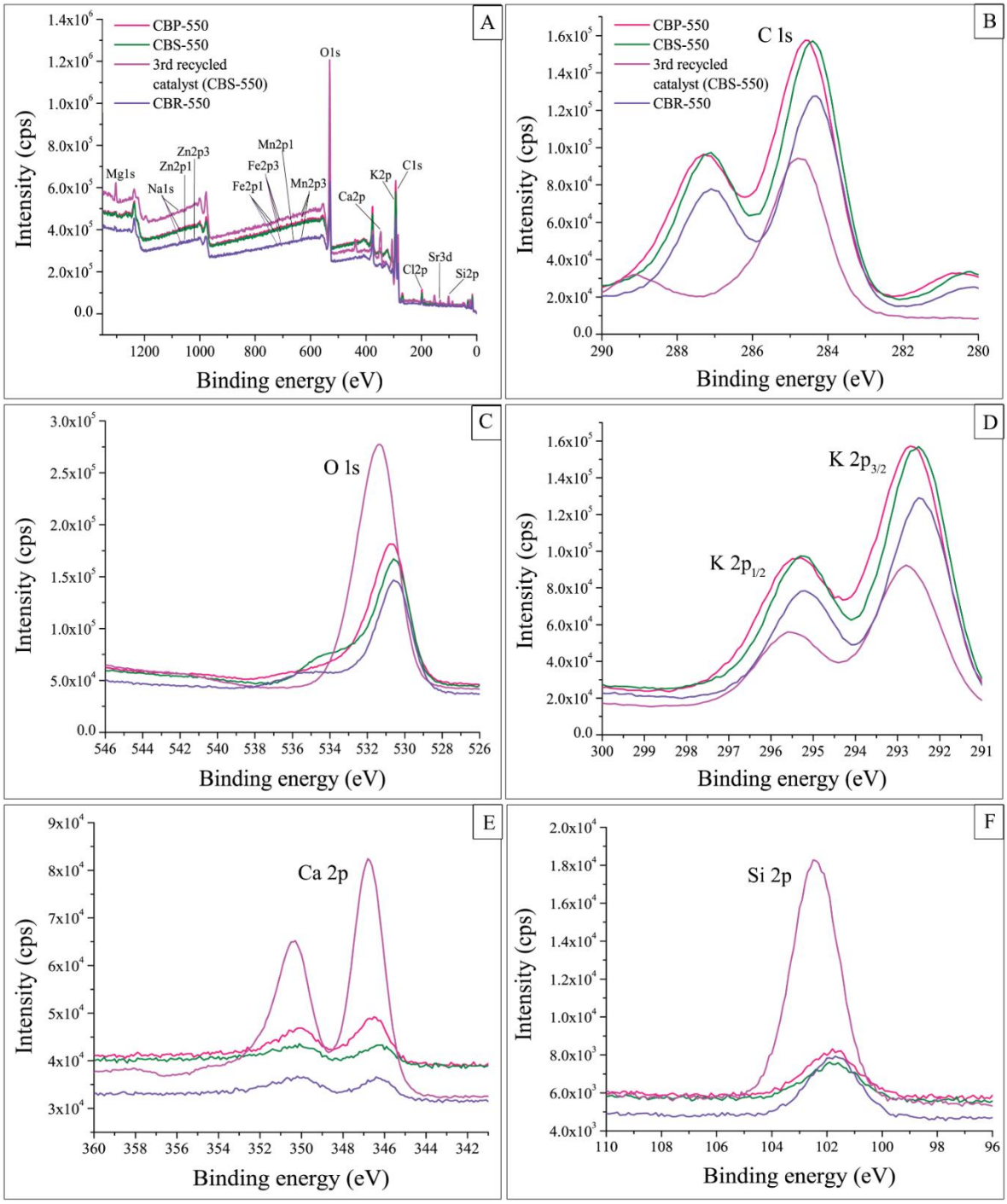

Fig. 5.10. XPS survey spectra (A) of CBP-550, CBS-550, CBR-550 and 3rd recycled catalysts; XPS patterns of C 1s (B), O 1s (C), K 2p (D), Ca 2p (E) and Si 2p (F).

Table 5.4: XPS analyses of burnt and calcined Bharatmoni catalysts.

Elements	**Composition of burnt Bharatmoni materials**			**Composition of catalyst calcined at 550 ºC**			
	BBP	**BBS**	**BBR**	**CBP-550**	**CBS-550**	**3rd recycled catalyst (CBS-550)**	**CBR-550**
	Atomic %	**Atomic %**	**Atomic %**	**Atomic %**	**Atomic %**	**Atomic %**	**Atomic %**
O1s	24.91	23.05	36.1	19.38	21.26	50.26	20.59
C1s	58.2	60.36	46.97	51.72	50.72	27.42	50.48
K2p	11.41	11.48	10.23	18.45	19.44	5.81	17.57
Ca2p	0.79	0.33	0.05	0.23	0.09	5.41	0.11
N1s	-	2.39	-	-	-	-	-
Na 1s	-	-	-	0.12	0.08	0.09	0.38
Mg1s	0.31	0.12	0.18	0.06	0.25	2.55	0.13
Mn2p	0.49	0.09	0.35	0.34	0.28	0.34	0.14
Fe2p	0.26	0.38	0.86	0.24	0.4	0.33	0.42
Zn2p	0.05	0.18	0.37	0.17	0.33	0.51	0.44
Si2p	1.45	-	3.3	6.13	4.17	5.42	7.43
Sr3d	0.98	0.4	0.35	0.27	0.63	1.26	0.66
Cl2p	1.15	0.63	1.03	2.9	2.33	0.61	1.65

5.3.1.7 Determination of pH values

The measured pH values of the present calcined catalysts are depicted in **Fig. 5.11**. In the ratio from 1:5 to 1:40 of catalyst weight by volume of distilled water (w/v), CBS-550 catalyst showed a higher pH value indicating highly basic. The root cause of the high basic character of the CBS-550 catalyst possibly due to the existence of higher compositions of potassium existing in the form of K_2CO_3 and K_2O as the basic active species. The high constituents of potassium, oxygen and carbon in the CBS-550 catalyst were supported by analyses results of EDX technique (**Table 5.2**) and XPS (**Table 5.4**). It is also found that the CBS-550 catalyst containing a high pH value showed the superior catalytic activity in this study. In other studies, the reported pH value of the base catalysts prepared from biomasses like *Sesamum indicum* (pH =11.4 at 1:10 w/v) (Nath et al., 2020) and *Brassica nigra* (pH = 11.91 at 1:5 w/v) (Nath et al., 2019) exhibited lower pH values than the current calcined catalysts.

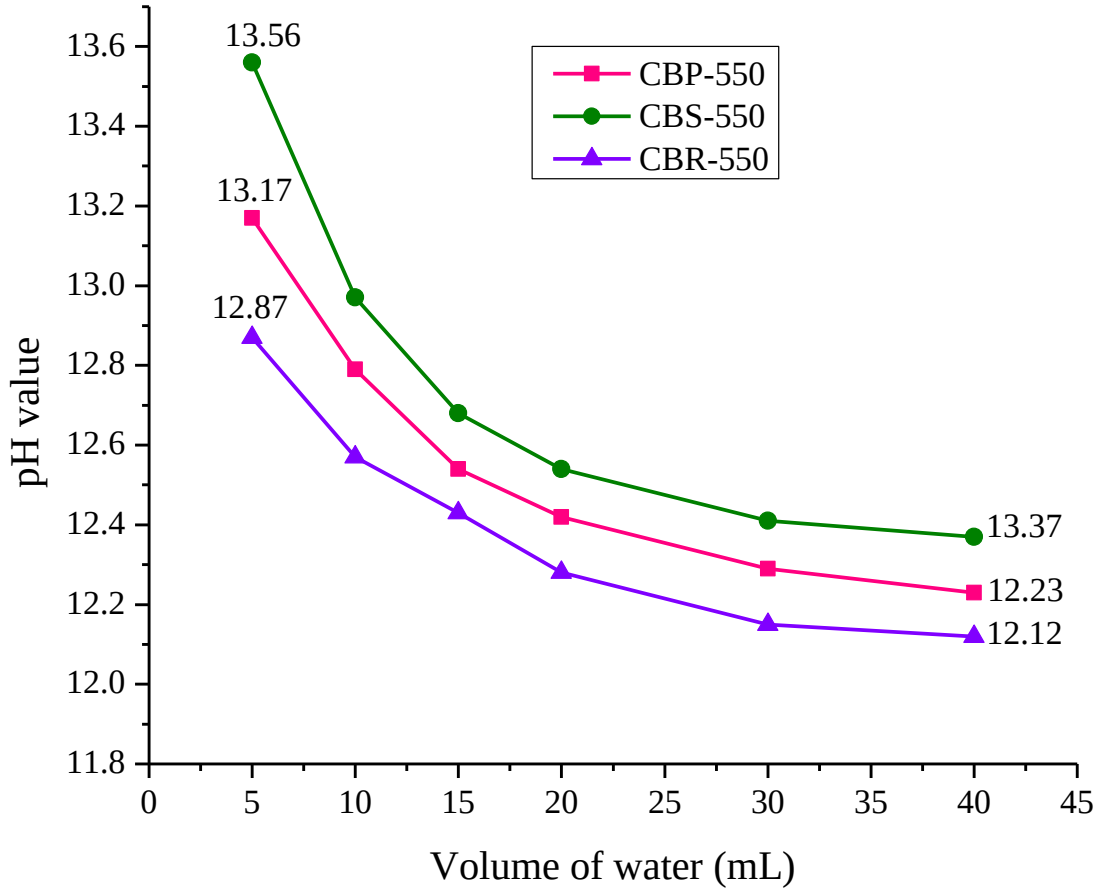

Fig. 5.11. Variation of pH values of calcined Bharatmoni catalysts (1 g) dissolved with different volume of water.

5.3.1.8 Soluble alkalinity, basicity and turnover frequency (TOF) studies

The determined values of soluble alkalinity of CBP-550, CBS-550 and CBR-550 were 5.31, 5.54 and 4.97 mmol g^{-1} respectively. It can be noticed that a higher soluble alkalinity value was found in the CBS-550 catalyst. The reason for higher soluble alkalinity may be due to the presence of an enormous amount of K and Ca in carbonate form which is supported by the analyses of FT-IR and XRD (Sharma et al., 2012; Mendonça et al., 2019b). Sharma et al. (2012) also tested soluble alkalinity and reported a higher value of 12.7 mmol g^{-1} for wood-based ash material showing good catalytic activity. The lower soluble alkalinity values were found by Mendonça et al. (2019a), Mendonça et al. (2019b) and Barros et al. (2020) for the catalysts prepared from peels of cupuaçu (1.05 mmol g^{-1}), tucumã (3.71 mmol g^{-1}) and pineapple leaves (0.39 mmol g^{-1}) respectively.

From the Hammett test, the basicity of CBP-550, CBS-550 and CBR-550 catalysts were measured as 1.36, 1.45 and 1.26 mmol g^{-1} respectively. The present Bharatmoni catalysts revealed the basic strength within the range $10.1 < H_- < 18.4$. CBS-550 catalyst has the highest

basicity and is because of the higher concentration of K constituted as carbonate and oxide along with other basic components like CaO and $CaCO_3$ (Daimary et al., 2022a). The abundance of basic sites is evident by the results of XPS, EDX and XRD analyses of this study. The lower basicity values were reported for barium cerate (1.74 mmol g^{-1}) (Sahani et al., 2019) and *Citrus sinensis* peel (0.170 mmol g^{-1}) (Changmai et al., 2021) catalysts which were also employed in the synthesis of biodiesel.

Based on the basicity values determined, the catalytic efficiencies concerning turnover frequency (TOF) of CBP-550, CBS-550 and CBR-550 catalysts were calculated. TOF measures the efficiency of a catalyst, which is one of the main parameters for commercial or industrial catalysts, and describes how many biodiesel molecules can be produced per unit of the basic active site and per unit of time (Roy et al., 2020c). The calculated TOF values of CBP-550, CBS-550 and CBR-550 catalysts were 7.98 h^{-1}, 10.03 h^{-1} and 7.66 h^{-1} respectively. The comparable TOF values were reported in *Musa chinensis* peel (16.85 h^{-1}) and trunk (7.025 h^{-1}) catalysts (Brahma et al., 2023). Roy et al. (2020c) reported a lower TOF value of 4.29 h^{-1} for the K-based lanthanum oxide employed as the catalyst in the biodiesel synthesis.

5.3.2 Role of Bharatmoni catalysts in the biodiesel synthesis

5.3.2.1 Effect of catalyst concentration

In this study, the CBS-550 catalyst loaded based on the *J. curcas* oil's weight in the reaction mixture of 9:1 MTOMR (methanol to oil molar ratio) and the reaction set up at 65 ^oC was investigated. The amount of catalyst loaded in the reaction is a significant parameter to attain the optimized condition for the production of biodiesel. The reactions loaded with 3, 5, 7 and 9 wt. % of the CBS-550 catalyst and its outcome with different biodiesel yields (%) produced at varying time periods are illustrated in **Fig. 5.12**. The reaction catalyzed by adding 3 and 5 wt. % of catalyst completed with a reduced reaction time from 26 min to 12 min with increasing biodiesel yield from 95.20 % to 96.97 % respectively (**Fig. 5.12**). The reason for reducing reaction time and increasing yield (%) with loading more catalyst is due to more abundant of basic active sites (Laskar et al., 2020). The biodiesel yield (%) is maximum in reaction loaded with 5 wt. % catalyst. The reaction loaded with 7 and 9 wt. % of the catalyst produced lower biodiesel yield (**Fig. 5.12**). This is because the reaction with a higher amount of catalyst that may worsen the mass transfer between the unmixable reactants by making the mixture more viscous leading to the hindrance of diffusion (Roy and Mohanty, 2021). Pathak et al. (2018), Oladipo et al. (2020), and Falowo and Betiku (2022) also reported from their studies that the biodiesel yield rises to a certain optimum amount of catalyst load and it was

known to drop with excessive catalyst load. Thus, the optimal catalyst dose for the present transesterification reaction is 5 wt. %.

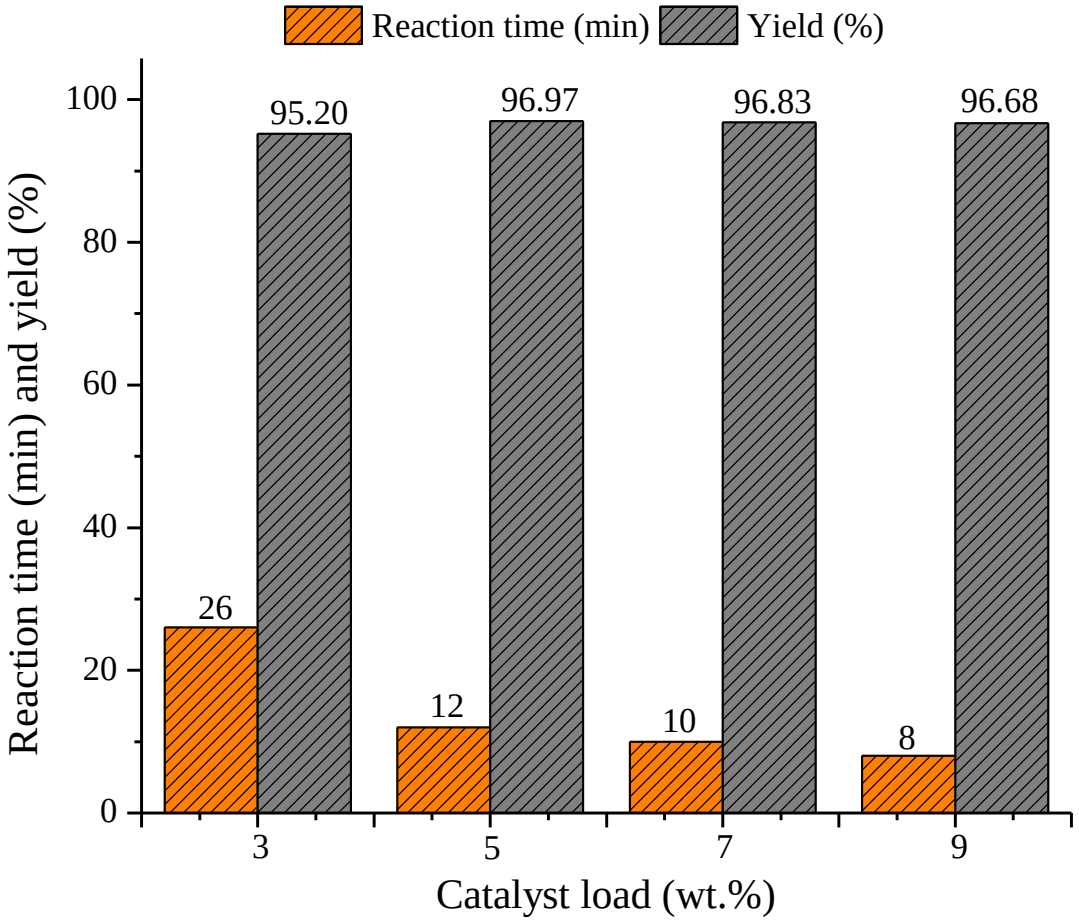

Fig. 5.12. Effect of catalyst loading of calcined Bharatmoni stem (CBS-550) on biodiesel synthesis (Temperature = 65 ^{o}C, MTOMR = 9:1).

5.3.2.2 Effect of MTOMR

MTOMR is one of the important factors that influence the biodiesel yield and reaction time of the reaction. Stoichiometrically, in a transesterification reaction, 3:1 MTOMR is required to synthesize 3 moles of methyl esters and one mole of glycerol. In this study, adding different MTOMRs ranging from 3:1 to 18:1 in the reaction using 5 wt. % of CBS-550 catalyst at 65 ^{o}C were investigated to obtain the optimum MTOMR and the results are represented in **Fig. 5.13**. When MTOMR was increased from 3:1 to 9:1, it was observed that the biodiesel yield increases from 94.69 % to 96.97 % along with a gradual reduction of reaction time from 19 min to 12 min. It can be explained that a larger volume of methanol than the required stoichiometric ratio can speed up the transesterification reaction. The excess methanol is essential to drive the reaction in the forward direction to maintain the equilibrium since the

transesterification reaction is reversible (Dhawane et al., 2016). Using MTOMR from 12:1 to 18:1, the biodiesel yield decreased from 96.86 % to 95.87 % with an increase in reaction time from 14 to 18 min (**Fig. 5.13**). The observed effect at large MTOMR is due to the fact that the reaction system gets diluted with excessive methanol and the catalyst's active sites on the surface get hampered which reduces the interaction between the triglyceride and catalyst and thus prevents the conversion of biodiesel. Furthermore, excessive methanol dissolves the byproduct glycerol which makes it difficult and lengthy to separate from biodiesel (Shan et al., 2015; Roy and Mohanty, 2021). Therefore, the optimum MTOMR determined for this work is 9:1.

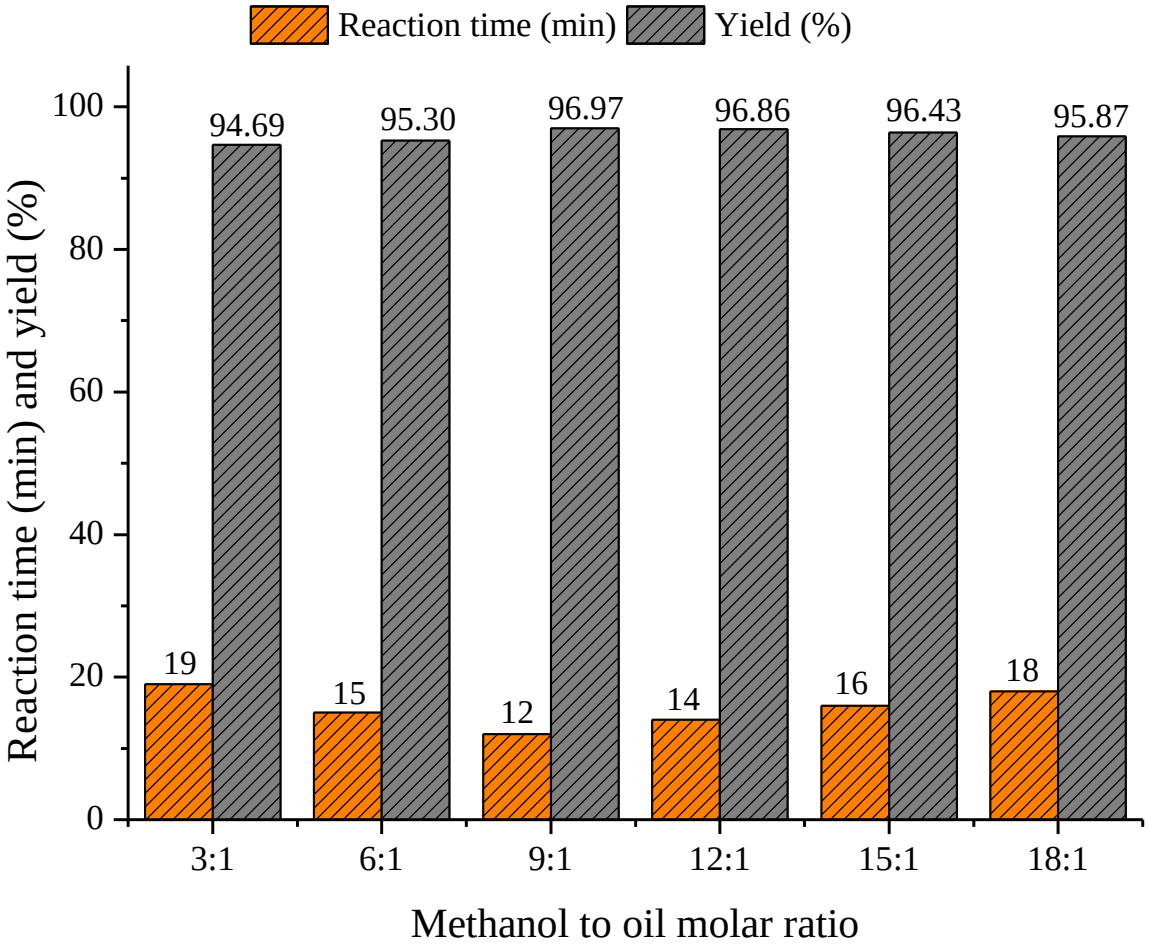

Fig. 5.13. Effect of MTOMR on biodiesel synthesis (Temperature = 65 ^{o}C, CBS-550 catalyst = 5 wt. %).

5.3.2.3 Effect of temperature

One of the most significant parameters that affect the transesterification is the temperature. In this study, the effect of temperature was investigated under the MTOMR of 9:1 and 5 wt. % of catalyst by utilizing the three calcined catalysts (CBP-550, CBS-550 and CBR-550). The experimental results are represented in **Fig. 5.14**. The experiments revealed that with rising temperatures from 35 ^{o}C to 75 ^{o}C the reaction time decreased. The improvement in the yield of biodiesel was noticed till the reaction temperature of 65 ^{o}C. All the examined reactions at 75 ^{o}C catalyzed by the three calcined catalysts showed no substantial improvement in biodiesel yield because methanol evaporates at 75 ^{o}C that possibly leads to the less interaction of the reaction mixture (Changmai et al., 2021; Madhuvilakku et al., 2013). Hence, the transesterification reaction at 65 ^{o}C catalyzed by the calcined catalysts showed the highest biodiesel yield in the order of CBS-550 (96.97 % in 12 min) > CBP-550 (96.89 % in 16 min) > CBR-550 (96.53 % in 18 min) (**Fig. 5.14)**. The efficiency of CBS-550 catalyst was found to be higher which agreed with the trends of higher potassium concentration (**Table 5.2**) and basic sites of the catalysts. The burnt ashes were also utilized to examine their activities at 65 ^{o}C and found that the BBS catalyst had yielded maximum biodiesel of 96.67 % in 25 min followed by BBP (96.19 % in 30 min) and BBR (95.73 % in 45 min) (**Fig. 5.15**). Among the burnt ash materials, the BBS catalyst showed higher catalytic activity that follows the trends of potassium concentration (**Table 5.1**). In this study, the reaction at 65 ^{o}C resulted in a maximum yield of 96.97 % within a short duration and hence this temperature is considered to be optimum.

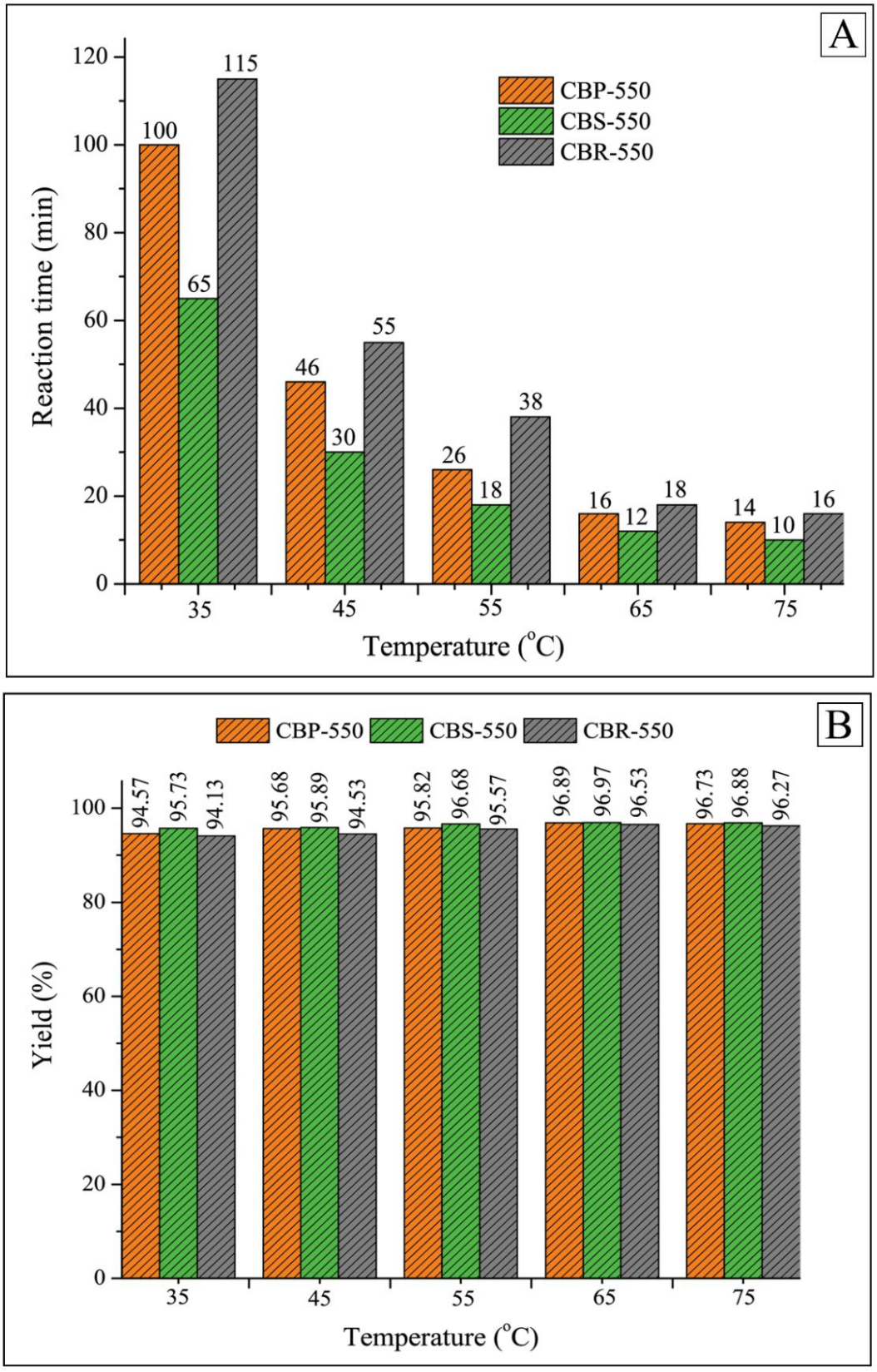

Fig. 5.14. Effect of temperature on biodiesel synthesis. Reaction conditions: MTOMR = 9:1, catalyst loading (CBP-550, CBS-550, CBR-550) = 5 wt. %.

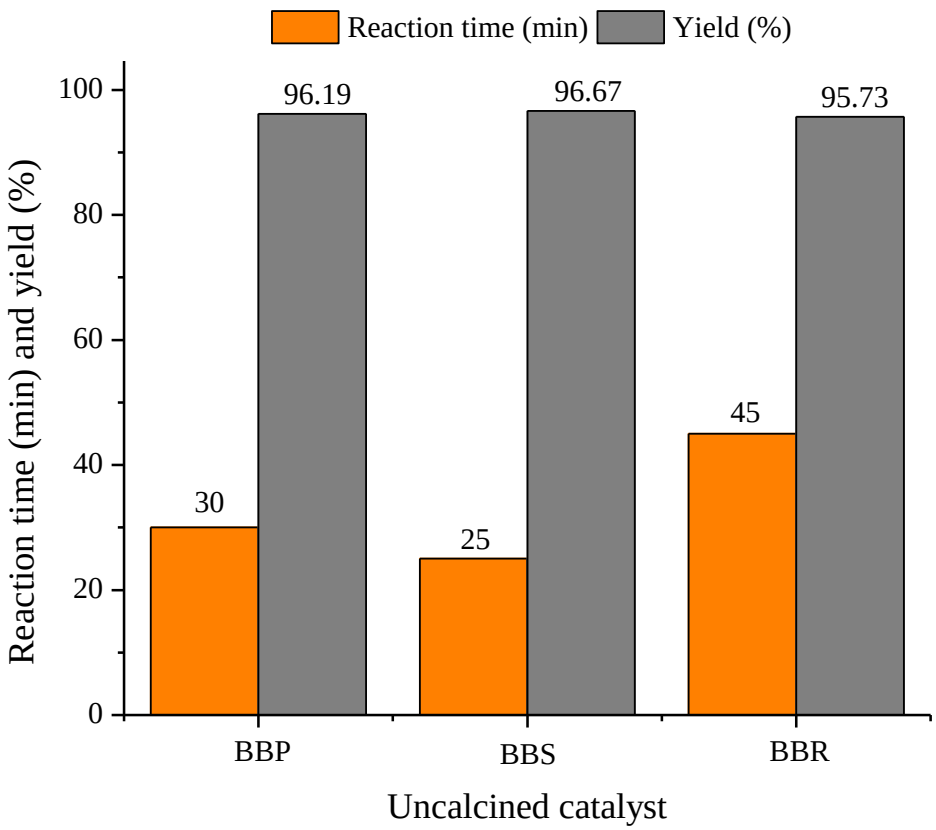

Fig. 5.15. Catalytic activities of the uncalcined Bharatmoni catalysts in biodiesel production. Reaction conditions: Temperature = 65 ^{o}C, MTOMR = 9:1, catalyst loading (BBP, BBS, BBR) = 5 wt. %.

5.3.2.4 Reusability of Bharatmoni catalyst

In this work, the reusability tests of the catalyst have been performed by utilizing the CBS-550 catalyst employing the optimum reaction parameters of 9:1 MTOMR and 5 wt. % catalyst amounts at 65 ^{o}C. A filtration process was carried out by using a suction pump to regenerate the fresh used catalyst from initial (first) reaction. It was then washed with petroleum ether 3-4 times to remove all the adhered substances (glycerol and methyl esters) from the catalyst. Thereafter, the recovered catalyst was taken in a petri-dish to dry at 110 ^{o}C for 4 h in a hot air oven following that, the catalyst was allowed to cool under a desiccator and reused for subsequent reactions up to 3rd cycle following a similar reaction and the catalyst separation procedures. It has been that the CBS-550 catalyst is effectively reusable up to the 3rd cycle revealing the reduction in catalytic activity and biodiesel yield after every subsequent cycle (**Fig. 5.16**). It is observed that the regenerated catalyst produced biodiesel of 95.67 % in 45 min (1st cycle), 94.43 % in 105 min (2nd cycle) and 93.20 % in 150 min (3rd cycle). This decline in catalytic activity is due to the leaching of active elements (Tarigan et al., 2022).

The catalyst sample regenerated after 3rd cycle was analyzed by FT-IR (**Fig. 5.3**), FESEM-EDX (**Fig. 5.7**) and XPS technique (**Table 5.4**). The FT-IR analysis revealed two new weak peaks at 2923 and 2854 cm^{-1} which are assigned to the C-H bond stretching indicating the contamination of the catalyst probably with glycerol or ester molecules and it causes the blockage of pores of the catalyst resulting in a declined catalytic activity (Daimary et al., 2022a). The morphological differences were noticed between the fresh catalyst sample (CBS-550) and the 3rd recycled catalyst (**Fig. 5.6** and **Fig. 5.7)**. The 3rd recycled catalyst has crushed cylindrical and oval shapes having its components washed out as compared to the structure of the fresh catalyst that has more aggregated components. EDX study revealed that 3rd recycled catalyst has a lower K concentration than the fresh CBS-550 catalyst (**Table 5.2**). The lowering of K concentration in the recovered catalyst was also detected in the XPS study (**Table 5.4**), which was primarily caused by the leaching out of the active components when the catalyst was reutilized for the 3rd reaction cycle (Rajkumari and Rokhum, 2020).

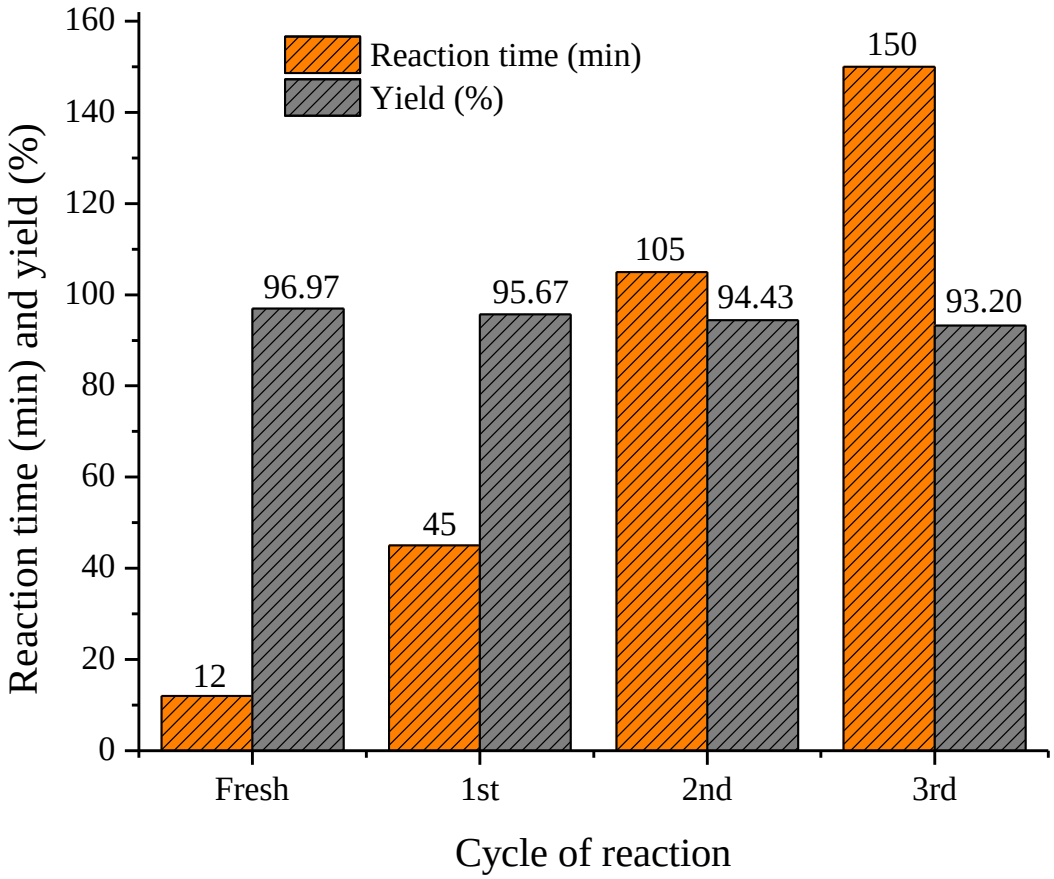

Fig. 5.16. Reusability of CBS-550 catalyst (Reaction temperature = 65 ^{o}C, MTOMR = 9:1, catalyst loading = 5 wt.%).

5.3.3 Kinetics study

The protocol of the kinetic study in this chapter is similar as described in the previous **Chapter 4** (**Section 4.3.3, Page no. 161**). In this work, kinetics studies of reactions for biodiesel production catalyzed by CBP-550, CBS-550 and CBR-550 catalysts were investigated. The reaction kinetics were determined with data achieved from the reactions performed under the optimized parameters, i.e loaded with 5 wt. % of catalyst and MTOMR of 9:1 at the reaction temperatures ranging from 35 to 75 ^{o}C (**Fig. 5.14**). Initially, the rate constants (k) were determined by substituting the required data in the standard kinetic equations as mentioned in the previous **Chapter 4 {Section 4.3.3, Page no. 162, Equation no. (4.5), (4.6), (4.7), and (4.8)}.**

The rate constants for various kinetic order reactions determined at various temperatures (in Kelvin, K) for the transesterification catalyzed by CBP-550, CBS-550 and CBR-550 catalysts are presented in **Tables 5.5, 5.6** and **5.7**. Using these data, Arrhenius plots for different orders of reactions are derived and can be visualized in **Fig. 5.17–5.20**. All the Arrhenius plots were linearly fitted to provide lines which was straight and the resultant correlation coefficients (R^2 value) as shown in **Tables 5.5, 5.6** and **5.7**. As a consequence of the linear graphs of all the reaction models, the one which is the best fit with the highest correlation coefficient value was selected to determine the specific reaction order (Yahya et al., 2018). By employing the CBR-550 catalyst, the reaction had the highest R^2 value of 0.95766 (**Table 5.7**) followed by the CBS-550 catalyst (R^2 value = 0.95033, **Table 5.6**) and CBP-550 catalyst (R^2 value = 0.94786, **Table 5.5**) and all of these belonged to the model of pseudo-first order reaction. Hence, it can be concluded that the current biodiesel production reaction catalyzed by the calcined Bharatmoni catalysts (CBP-550, CBS-550 and CBR-550) is following the kinetic model of pseudo-first order reaction. These results were found similar in the works of Kaur et al. (2018), Farid et al. (2018), Yahya et al. (2018) and Nath et al. (2023) reporting that the synthesis of biodiesel with addition of excessive of methanol followed the pseudo-first order kinetics.

The activation energies (E_a) were calculated by applying the slope = E_a/R obtained from respective Arrhenius plots (**Fig. 5.17–5.20**) (R = 8.314 J K^{-1} mol^{-1}) and the pre-exponential factor (A) values were also evaluated from the intercept (ln A) of the plots (**Fig. 5.17–5.20**). The calculated E_a and A values can be seen in **Tables 5.5, 5.6** and **5.7**. Based on the kinetic model of pseudo-first order, the reaction catalyzed by the CBS-550 catalyst has the lowest E_a value (44.36 kJ mol^{-1}) than CBP-550 (48.56 kJ mol^{-1}) and CBR-550 (49.26 kJ mol^{-1}) catalysts. This result supports that the CBS-550 catalyst has the highest catalytic activity among the

other two catalysts of this study (CBP-550 and CBR-550), and the E_a was also achieved in the stated range of 21–84 kJ mol^{-1} for the reactions of biodiesel syntheses (Yahya et al; 2018; Kaur et al., 2018; Nath et al., 2023). According to this study, CBP-550, CBS-550 and CBR-550 catalyzed reactions have lower E_a values than the values reported by Mendonça et al. (2019b) (61.23 kJ mol^{-1}) and Nath et al. (2023) (50.63 kJ mol^{-1}) in their studies indicating the superiority of the present catalyst.

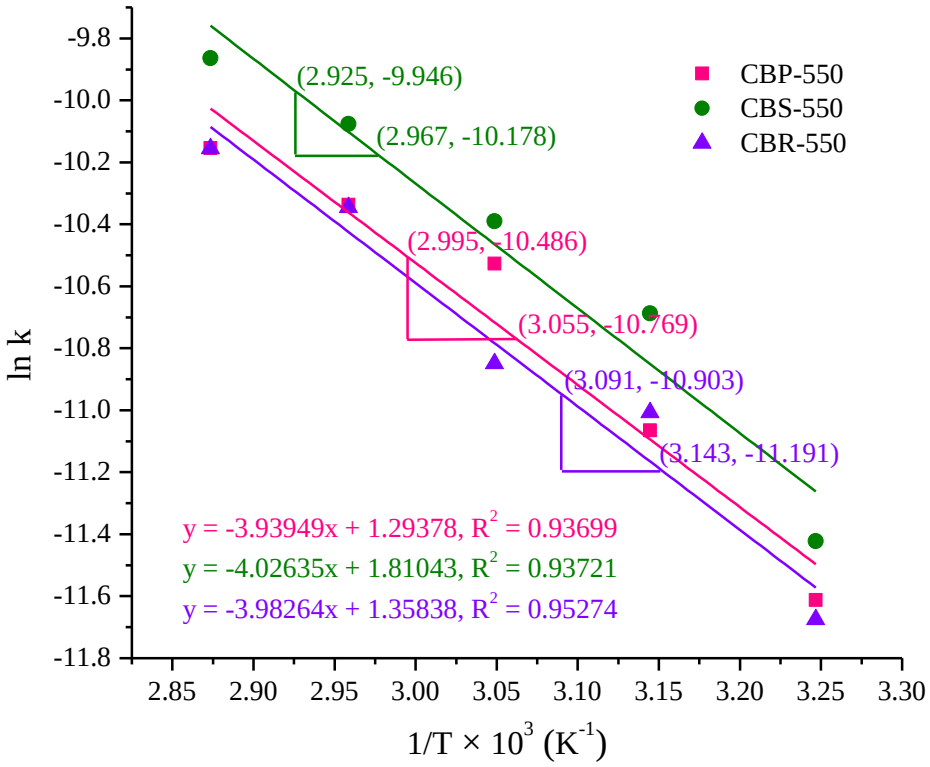

Fig. 5.17. Arrhenius plot (ln k versus $1/T \times 10^3$) for the reaction of zero-order rate model employing Bharatmoni catalysts (Reaction temperatures = 35, 45, 55, 65 and 75 °C).

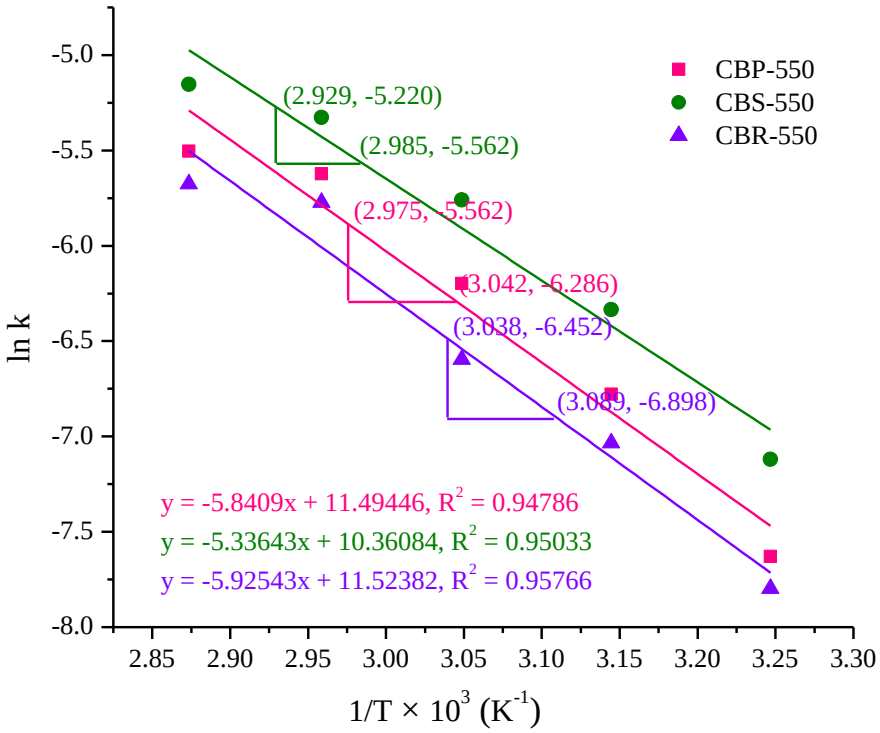

Fig. 5.18. Arrhenius plot (ln k versus $1/T \times 10^3$) for the reaction of pseudo-first order rate model employing Bharatmoni catalysts (Reaction temperatures = 35, 45, 55, 65 and 75 ^oC).

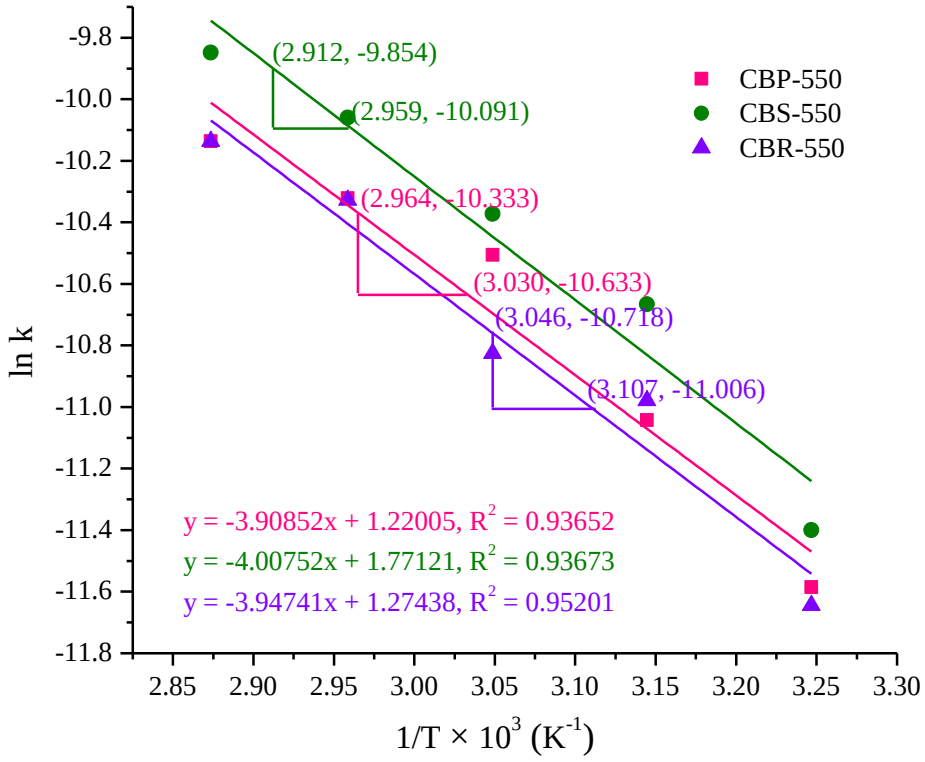

Fig. 5.19. Arrhenius plot (ln k versus $1/T \times 10^3$) for the reaction of first order rate model employing Bharatmoni catalysts (Reaction temperatures = 35, 45, 55, 65 and 75 ^oC).

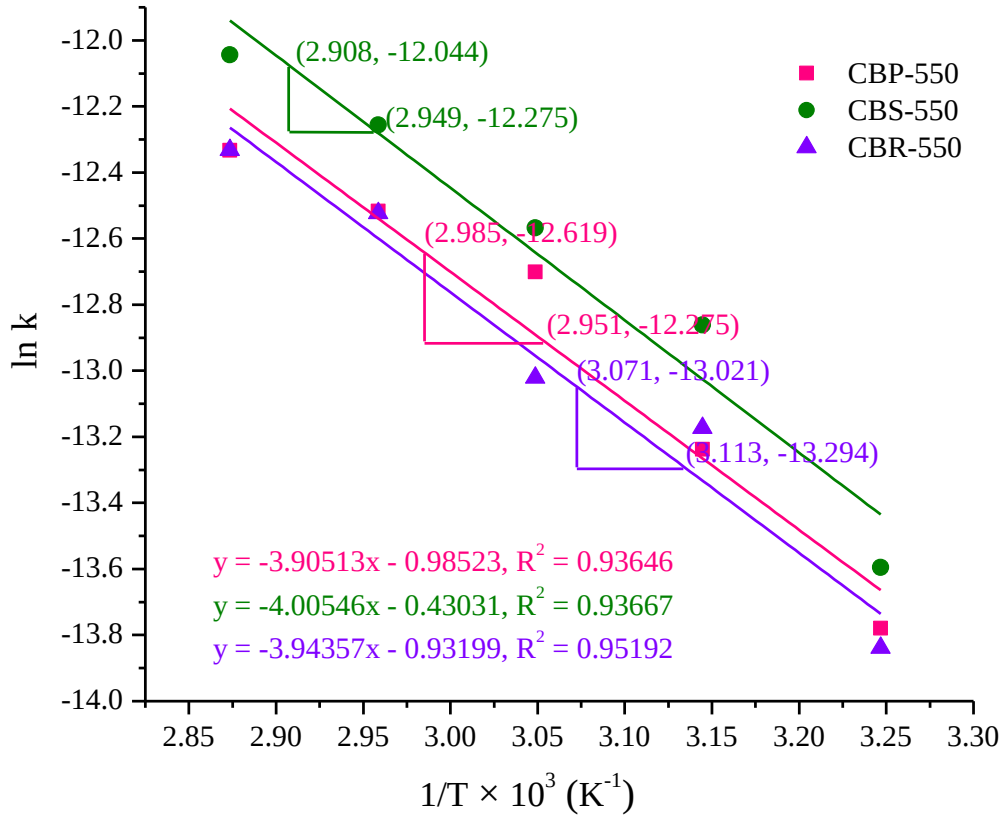

Fig. 5.20. Arrhenius plot (ln k versus $1/T\times10^3$) for the reaction of second order rate model employing Bharatmoni catalysts (Reaction temperatures = 35, 45, 55, 65 and 75 ^oC).

Table 5.5: Rate constant (k), correlation coefficient (R^2), activation energy (E_a) and pre-exponential factor (A) of various kinetic models of the reaction catalyzed by CBP-550 catalyst.

Order of reaction	**Rate constant, k (s^{-1}) at various temperature (K)**					**R^2 value**	**Activation energy, E_a (kJ mol^{-1})**	**Pre-exponential factor, A (s^{-1})**
	308	**318**	**328**	**338**	**348**			
Zero order	9.05×10^{-6}	1.57×10^{-5}	2.68×10^{-5}	3.24×10^{-5}	3.89×10^{-5}	0.93699	32.75	3.65
First order	9.31×10^{-6}	1.60×10^{-5}	2.74×10^{-5}	3.29×10^{-5}	3.96×10^{-5}	0.93652	32.49	3.39
Pseudo-first order	4.86×10^{-4}	1.14×10^{-3}	2.04×10^{-3}	3.62×10^{-3}	4.07×10^{-3}	0.94786	48.56	9.82×10^4

Second order	1.03×10^{-6}	1.78×10^{-6}	3.04×10^{-6}	3.66×10^{-6}	4.40×10^{-6}	0.93646	32.46	3.73×10^{-1}

Table 5.6: Rate constant (k), correlation coefficient (R^2), activation energy (E_a) and pre-exponential factor (A) of various kinetic models of the reaction catalyzed by CBS-550 catalyst.

Order of reaction	**Rate constant, k (s^{-1}) at various temperature (K)**					**R^2 value**	**Activation energy, E_a (kJ mol^{-1})**	**Pre-exponential factor, A (s^{-1})**
	308	**318**	**328**	**338**	**348**			
Zero order	1.09×10^{-5}	2.28×10^{-5}	3.07×10^{-5}	4.21×10^{-5}	5.20×10^{-5}	0.93721	33.47	6.11
First order	1.12×10^{-6}	2.33×10^{-5}	3.13×10^{-5}	4.27×10^{-5}	5.28×10^{-5}	0.93673	33.31	5.88×10^{4}
Pseudo-first order	8.09×10^{-4}	1.77×10^{-3}	3.15×10^{-3}	4.86×10^{-3}	5.78×10^{-3}	0.95033	44.36	3.16×10^{4}
Second order	1.25×10^{-6}	2.60×10^{-6}	3.48×10^{-6}	4.76×10^{-6}	5.88×10^{-6}	0.93667	33.30	6.50×10^{-1}

Table 5.7: Rate constant (k), correlation coefficient (R^2), activation energy (Ea) and pre-exponential factor (A) of various kinetic models of the reaction catalyzed by CBR-550 catalyst.

Order of reaction	**Rate constant, k (s^{-1}) at various temperature (K)**					**R^2 value**	**Activation energy, E_a (kJ mol^{-1})**	**Pre-exponential factor, A (s^{-1})**
	308	**318**	**328**	**338**	**348**			
Zero order	8.51×10^{-6}	1.66×10^{-5}	1.94×10^{-5}	3.21×10^{-5}	3.89×10^{-5}	0.95274	33.11	3.89
First order	8.77×10^{-6}	1.70×10^{-5}	1.99×10^{-5}	3.27×10^{-5}	3.96×10^{-5}	0.95201	32.81	3.58

Pseudo-first order	4.11×10^{-4}	8.81×10^{-4}	1.37×10^{-3}	3.11×10^{-3}	3.43×10^{-3}	0.95766	49.26	1.01×10^{5}
Second order	9.78×10^{-7}	1.90×10^{-6}	2.21×10^{-6}	3.64×10^{-6}	4.41×10^{-6}	0.95192	32.78	3.94×10^{-1}

5.3.4 Study of thermodynamic properties of the reaction

In this study, the thermodynamic properties such as a change in enthalpy (ΔH), entropy (ΔS) and Gibbs free energy change (ΔG) of the reactions catalyzed by CBP-550, CBS-550 and CBR-550 catalysts were calculated by using the similar standard equations described in **Chapter 4** (**Section 4.3.4, Page no. 165**).

The determined ΔH values were found to be + 45.84, + 41.64 and + 46.54 kJ mol^{-1} K^{-1} for the reactions catalyzed by CBP-550, CBS-550 and CBR-550 catalysts, respectively (**Table 5.8**). Consequently, these positive values of the ΔH explain that the reaction takes place through an endothermic process and requires external heat to proceed (Nath et al., 2023). Sarve et al. (2016) and Nath et al. (2023) also stated the positive ΔH values for biodiesel production via the transesterification process explaining that their reactions were endothermic in nature too. In the present work, the determined ΔS values were found to be negative ($\Delta S < 0$) as shown in (**Table 5.8**) which indicates that the randomness occurring during the reaction is less (Roy et al., 2020a). The calculated ΔG values (**Table 5.8)** for the reactions experimented at different temperatures show that the obtained results are all positive ($\Delta G > 0$). This positive value describes that the reactions catalyzed by the present catalysts are non-spontaneous and endergonic reactions (Nath et al., 2023).

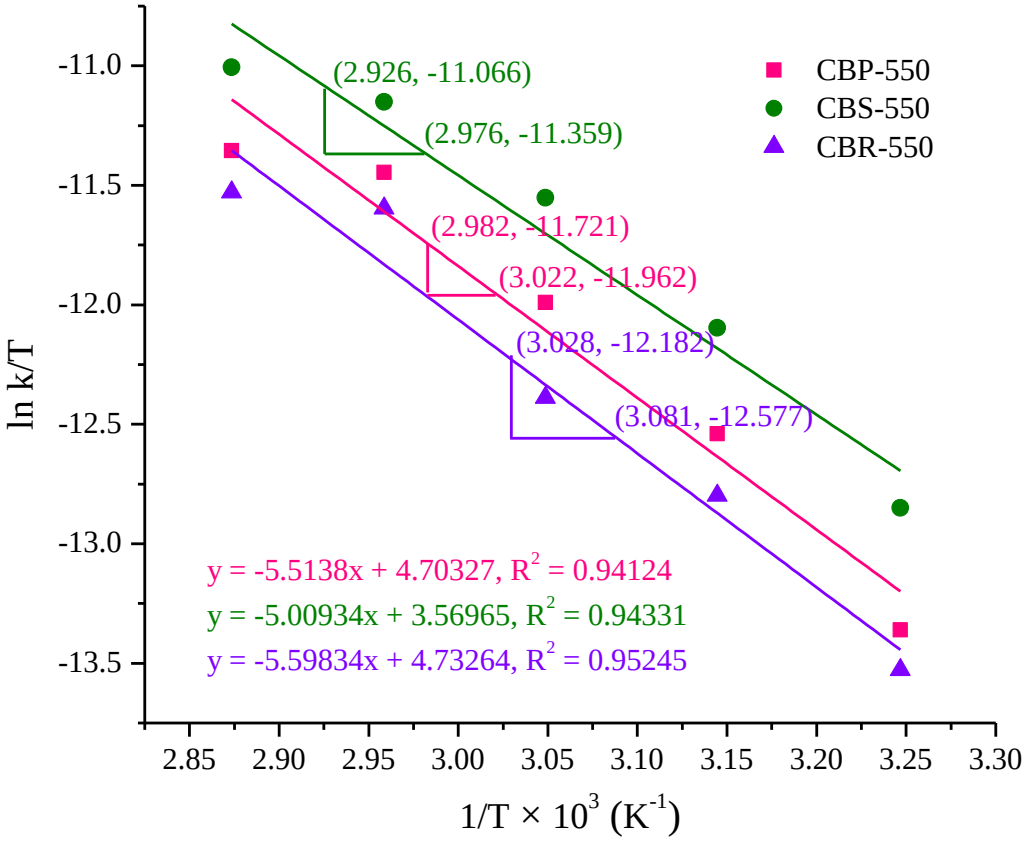

Fig. 5.21. Eyring-Polanyi plot (ln k/T versus $1/T\times10^3$) for the study of thermodynamic properties of the reaction employing the Bharatmoni catalysts.

Table 5.8: Thermodynamic properties of the reaction catalyzed by CBP-550, CBS-550 and CBR-550 catalysts.

Catalysts	**Thermodynamic properties**						
	ΔH (kJ mol^{-1} K^{-1})	**ΔS (kJ mol^{-1} K^{-1})**	**ΔG (kJ mol^{-1})**				
			308 K	**318 K**	**328 K**	**338 K**	**348 K**
CBP-550	45.84	-1.039	727.45	376.25	386.64	397.03	407.42
CBS-550	41.64	-1.048	364.57	375.05	385.54	396.02	406.51
CBR-550	46.54	-1.038	366.49	376.88	387.26	397.65	408.04

5.3.5 Comparison of Bharatmoni catalysts with other biomass-based catalysts.

In this work, the performances of CBP-550, CBS-550 and CBR-550 catalysts are compared with other reported catalysts and summarized in **Table 5.9**. Under the optimum experimental conditions (5 wt.%, 9:1, 65 ^{o}C), the present study disclosed that the utilization of CBP-550, CBS-550 and CBR-550 catalysts in the reaction produced the highest biodiesel yield of 96.89 %, 96.97 %, and 96.53 %, respectively in short reaction time. Sarma et al. (2014) and Aslam et al. (2014) experimented setting out a transesterification reaction at a very high temperature (275 ^{o}C) from which they achieved 98 % yield in 60 min and 95 % conversion in 60 min respectively. Considering the energy input and reaction time, their catalysts are less effective than the current catalysts. Likewise, Laskar et al. (2018) and Changmai et al. (2021) also reported higher duration of reaction that might be due to the lower basic strength of their catalysts in comparison to the current catalysts. There are some works on the production of biodiesel from variety of oil feedstocks applying solid base catalysts producing higher biodiesel yield than this work but reported longer reaction completion time, for example, Daimary et al. (2022a) achieved 98 % in 120 min, Eldiehy et al. (2022) obtained 98 % of biodiesel in 120 min, Daimary et al. (2022b) reported 97.5 conversion in 120 min and Nath et al. (2020) also reported 98.9 % yield in 40 min (**Table 5.9**). So, the present calcined catalysts are revealed to be better at synthesizing biodiesel faster than their catalysts. The present calcined catalysts have better catalytic activity than the catalysts studied by Tarigan et al. (2022), Oladipo et al. (2020), Sharma et al. (2012), Aleman-Ramirez et al. (2021), Chouhan and Sarma (2013) because their catalysts achieved lower biodiesel yield or conversion with longer reaction time. Niju et al. (2021), Etim et al. (2021), Basumatary et al. (2021c), Balajii and Niju (2020), and Changmai et al. (2020b) have reported lower potassium contents causing less catalytic activity. Nath et al. (2023) reported comparable catalytic activity, their catalysts also exhibited high basic in nature due to the presence of high concentration of alkali metal carbonates and oxides. Although present catalysts have a lower surface area than the other biomass-based catalysts mentioned in **Table 5.9**, it has superior catalytic activity because of the high concentration of potassium and more basic nature. Thus, present catalysts (CBP-550, CBS-550 and CBR-550) have a significant capacity for catalyzing the transesterification for faster production of biodiesel.

Table 5.9: Catalytic activities of Bharatmoni catalysts and their comparison in biodiesel syntheses with other reported solid catalysts derived from waste biomass.

Biodiesel feedstock	**Catalyst**	**Surface area ($m^2 g^{-1}$)**	**Parameters**				**Biodiesel, Y or C (%)**	**References**
			MTOMR	**Catalyst (wt. %)**	**Temp (°C)**	**Time (min)**		
J. curcas oil	CBP-550 (peel)	2.061	9:1	5	65	16	96.89 (Y)	This study
J. curcas oil	CBS-550 (Stem)	0.730	9:1	5	65	12	96.97 (Y)	This study
J. curcas oil	CBR-550 (rhizome)	0.857	9:1	5	65	18	96.53 (Y)	This study
J. curcas oil	MBUS	38.7	9:1	5	275	60	98 (Y)	Sarma et al. (2014)
Mesua ferrea oil	MBUS	38.7	9:1	5	275	60	95 (C)	Aslam et al. (2014)
WCO	Sweet potato leaves	2.81	9:1	5	60	120	98.0 (C)	Eldiehy et al. (2023)
WCO	Potato peel	23.5	9:1	3	60	120	97.5 (C)	Daimary et al. (2022b)
J. curcas oil	*Musa champa peduncle*	8.57	12:1	7	65	6	98.23 (Y)	Nath et al. (2023)
Palm oil	Passion fruit peel	-	15:1	7	RT	30	95.4 (Y)	Tarigan et al. (2022)
Soybean oil	Snail shell	7.0	6:1	3	28	420	98 (Y)	Laskar et al. (2018)
WCO	*Citrus sinensis* peel ash@Fe_3O_4	15.55	6:1	6	65	180	98 (Y)	Changmai et al. (2021)
WCO	*Musa acuminata* peel	12	9:1	1.5	60	120	98 (Y)	Daimary et al. (2022a)

Sunflower oil	*Sesamum indicum*	3.66	12:1	7	65	40	98.9 (Y)	Nath et al. (2020)
Moringa oleifera oil	Pawpaw peel	3.6	9:1	3.5	35	40	96.43 (Y)	Oladipo et al. (2020)
J. curcas oil	$CaCO_3$-*Acacia nilotica* ash	14.0	12:1	5	65	180	91.7 (C)	Sharma et al. (2012)
Soybean oil	*Moringa oleifera* leaves	–	6:1	6	65	120	86.7 (Y)	Aleman-Ramirez et al. (2021)
J. curcas oil	*Lemna perpusilla*	9.6	9:1	5	65	300	89.43 (Y)	Chouhan and Sarma (2013)
Madhuca indica oil	Poovan banana pseudostem	4.58	14.9:1	5.9	65	178	97.97 (C)	Niju et al. (2021)
Used vegetable oil	*Carica papaya* peel	–	12:1	3.5	65	60	97.5 (Y)	Etim et al. (2021)
J. curcas oil	*Heteropanax fragrans*	27.50	12:1	7	65	65	97.75 (Y)	Basumatary et al. (2021c)
Ceiba pentandra oil	MA peduncle	45.9	11.46:1	2.68	65	106	98.73 (C)	Balajii and Niju (2020)
Soybean oil	Orange peel ash	605.60	6:1	7	RT	420	98 (C)	Changmai et al. (2020b)

Wt–weight; min–minute; Y–yield; Temp–temperature; C–conversion; MTOMR – Methanol to oil molar ratio; WCO–Waste cooking oil; MB–*Musa balbisiana*; MBUS–*Musa balbisiana* underground stem; MA–*Musa acuminate*.

5.3.6 FTIR, NMR and GC-MS analyses

The FT-IR analyzed spectra for *J. curcas* oil and produced biodiesel are displayed in **Fig. 5.22**. The strong absorption peak at 1746 cm^{-1} is attributed to the stretching frequency of C=O group of the glyceride in oil. The existence of methyl ester in the present biodiesel sample was characterized by the strong absorption peak of C=O stretching frequency at 1740 cm^{-1} which is a significant implication of the successful conversion of *J. curcas* oil into FAME (Basumatary et al., 2021c). Both for oil and biodiesel, the band at 3461 cm^{-1} with weak intensity is belonging to -C=O overtone and the peak located at 3005 cm^{-1} is due to =C-H stretching vibration (Falowo et al., 2020). The bands at 2928 cm^{-1} and 2853 cm^{-1} indicated the =C-H asymmetric and $–CH_2$ symmetric stretching vibrations respectively (Dharma et al., 2016). The peaks of shear-type vibration of $–CH_2$ with moderate intensity are also recognized for oil at 1462 cm^{-1} and biodiesel at 1462 and 1434 cm^{-1}. Besides that, CH_3 bending vibration displays the peaks at 1372 and 1241 cm^{-1} for oil and at 1366 and 1248 cm^{-1} for biodiesel (Dharma et al., 2016; Falowo et al., 2020). The peaks for oil at 1165 and 1096 cm^{-1} and biodiesel at 1199, 1171, and 1019 cm^{-1} indicate the anti-symmetric stretching vibrations of C-O-C. It is evident that $–CH_2–$ plane rocking of long chains of fatty acids is responsible for the peak exhibiting at 722 cm^{-1} both for oil and the produced biodiesel (Dharma et al., 2016). The study exposed the transformation of *J. curcas* oil into biodiesel by revealing the above-mentioned remarkable peaks. The ^{1}H-NMR spectroscopic analysis result of *J. curcas* biodiesel of this work is displayed in **Fig. 5.23**. The various protons revealed by the ^{1}H-NMR analysis at different chemical shifts can be observed, more significantly the signal appearing at δ 3.592 ppm interpreted the formation of methoxy proton ($-COOCH_3$) of esters that was found in the sample of produced biodiesel. Generally, methine proton (-CH-) at C2 of glycerides ($-CH-CO_2R$) and methylene protons ($-CH_2-$) at C1 and C3 of glycerides ($-CH_2-CO_2R$) can be found in triglyceride whereas methoxy protons of ester groups do not exist in triglyceride (Basumatary et al., 2021a; Basumatary et al., 2023; Nath et al., 2023). The methine proton and methylene protons were not found by the ^{1}H-NMR spectrum of biodiesel. Thus, the formation of a singlet signal for the existence of methoxy protons in the biodiesel of this work confirmed that *J. curcas* oil is successfully converted to biodiesel after transesterification. From the analyzed GC chromatograms (**Fig. 5.24**) and following the library search with TurboMass software, the FAME profiles that existed in the transformed biodiesel are shown in **Table 5.10**. The analysis result confirmed that the produced biodiesel has methyl oleate (41.326 %), methyl palmitate (20.105 %), and methyl linoleate (17.883 %) as major components along with methyl stearate

(4.831 %), methyl arachidate (1.290 %), methyl gondoate (0.848 %) and methyl lignocerate (0.177 %) as minor components.

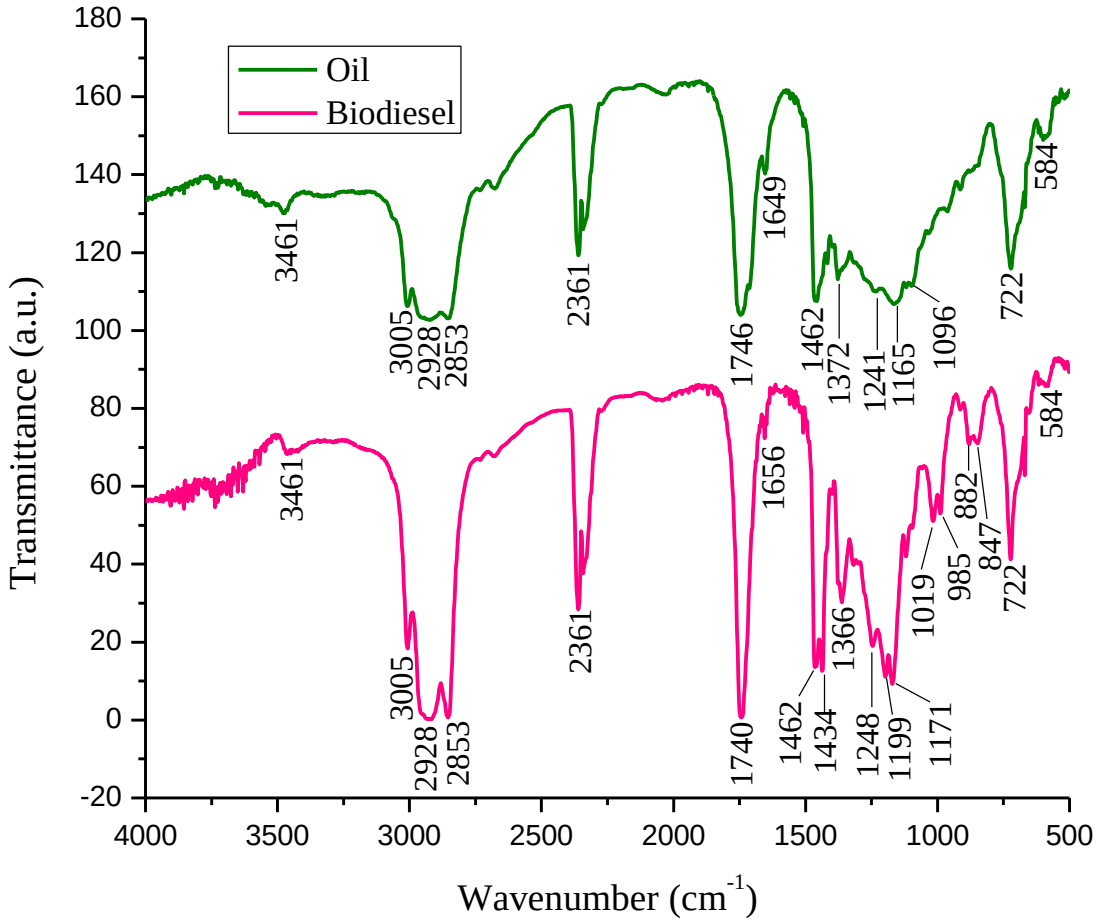

Fig. 5.22. FT-IR spectra of *J. curcas* oil and its biodiesel.

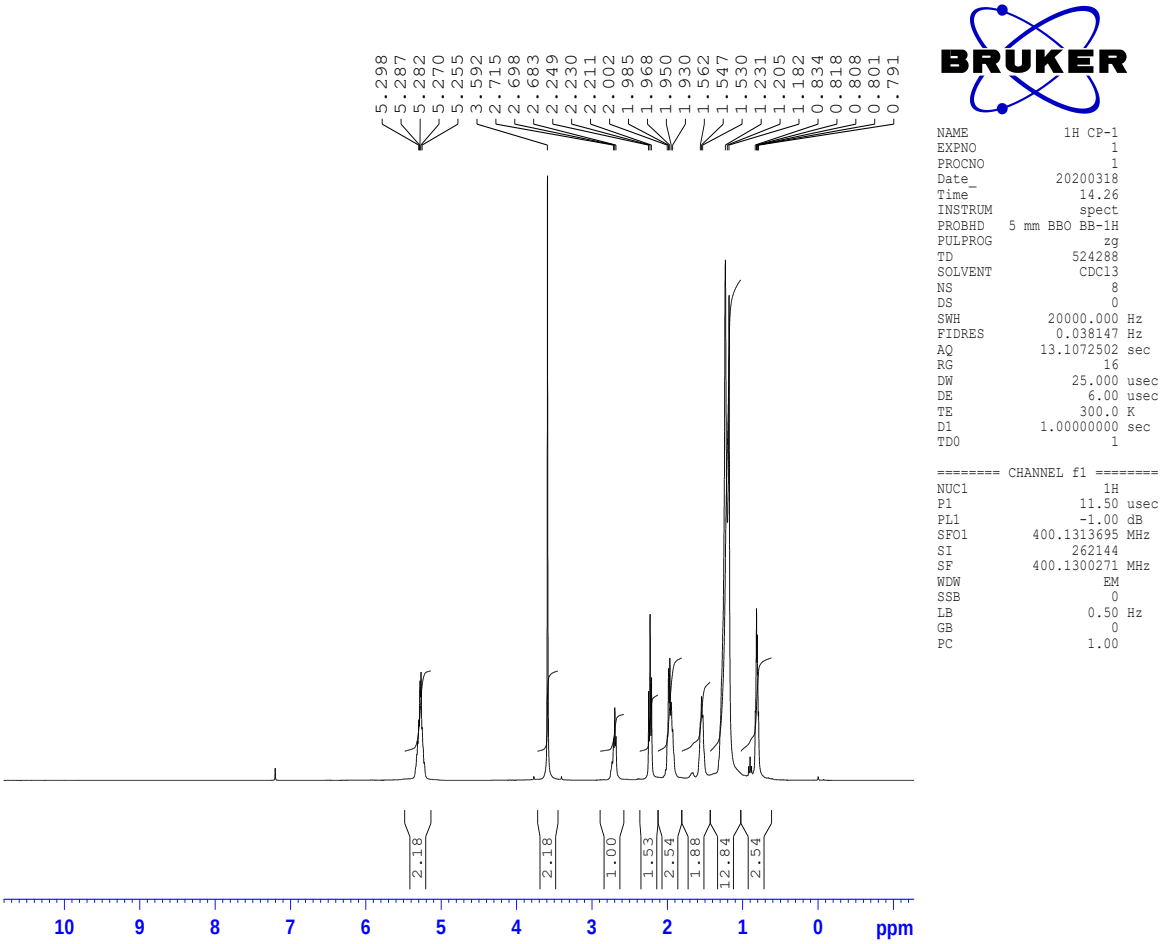

Fig. 5.23. ^{1}H NMR spectrum of *J. curcas* biodiesel.

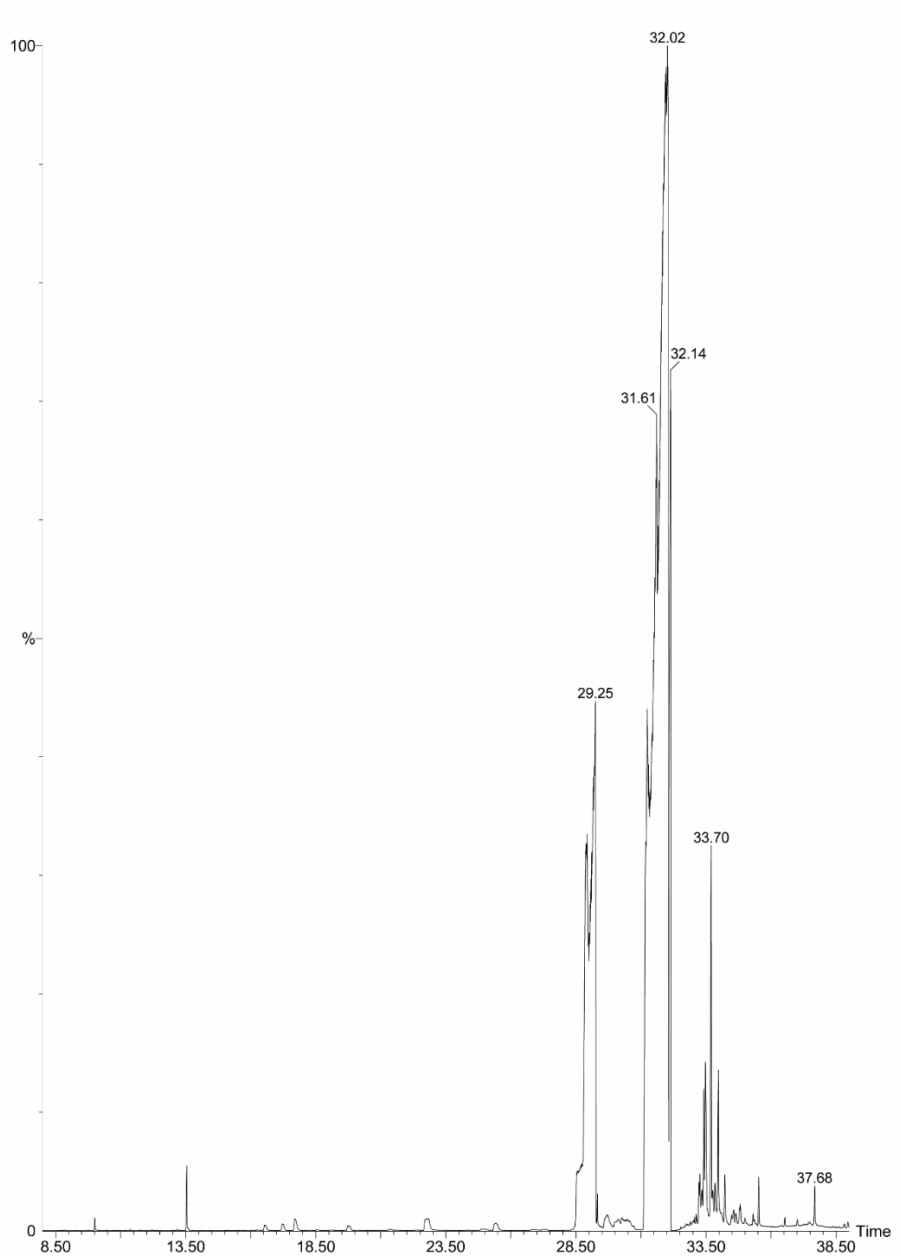

Fig. 5.24. GC-MS of *J. curcas* biodiesel.

Table 5.10: Chemical compositions of *J. curcas* biodiesel from GC-MS analysis.

RT	FAME	Composition (%)
29.25	Methyl palmitate [C16:0]	20.105
31.61	Methyl linoleate [C18:2]	17.883
32.02	Methyl oleate [C18:1]	41.326
32.14	Methyl stearate [C18:0]	4.831
33.47	Methyl gondoate [C20:1]	0.848
33.70	Methyl arachidate [C20:0]	1.290
37.68	Methyl lignocerate [C24:0]	0.177

5.3.7 Physicochemical properties of biodiesel

The physicochemical properties of the generated biodiesel in this work were analyzed and compared with other biodiesel and international standards set by ASTM D6751 and EN 14214 (**Table 5.11)**. The determined AV and FFA of the oil were found to be 9.2 mg KOH/g and 4.6 mg KOH/g respectively. This feedstock oil was utilized to synthesize biodiesel through direct transesterification without pre-treatment or esterification. The AV and FFA of the produced biodiesel showed 0.36 mg KOH/g and 0.18 mg KOH/g respectively. This AV and FFA value of the produced biodiesel is within the maximum limits (0.5 mg KOH/g) prescribed by international standard EN 14214. Chouhan and Sarma (2013) and Taufiq-Yap et al. (2014) also reported the direct transesterification of *J. curcas* oil into biodiesel without pretreatment having AV of 7.46 and 13.60 mg KOH/g respectively. This study obtained the density of biodiesel as 0.8757 g/cm^3 at 15 ^{o}C, which is within the range of standard values and well compared to other results mentioned in **Table 5.11**. Thus, in terms of density, the produced biodiesel is preferable since the density also determines how much fuel is required to generate particular engine power based on its density (Balaji and Niju, 2020). For biodiesel to flow smoothly through an engine, its kinematic viscosity is responsible and the value obtained for the present biodiesel is 4.027 mm^2/s at 40 ^{o}C which meets the value of the international standard. This value is lower than the kinematic viscosity value determined by Chouhan and Sarma (2013) and Olatundun et al. (2020) which means the present fuel has better combustion characteristics without deposition in the engine than their studies (Basumatary et al., 2021c). The cetane number was obtained to be 50.3, it is above the minimal value specified by ASTM D6751 and slightly greater than the cetane number of biodiesels reported by Sarma et al. (2014) and Kumar et al. (2016). The calculated cetane index for the present biodiesel is 57.58. In this study, the significant fuel property like pour point and cold filter plugging point (CFPP) of biodiesel were computed to be 0 ^{o}C and < 4 ^{o}C respectively. The saponification number (SN) was determined to be 191.28 (mg KOH/g) that expresses saponifiable unit per unit weight of *J. curcas* biodiesel. The iodine value representing the unsaturation degree was observed to be 76.70 g I_2/100 g which is below the stated limit of EN 14214 standard and nearly the same values were reported by Olatundun et al. (2020) and Falowo and Betiku (2022), but Sarma et al. (2014) achieved higher iodine value. The determined value of the diesel index, American petroleum index (API), and aniline point for the biodiesel produced in this work were recorded as 66.08, 34.28, and 192.77 respectively. The energy content in the present biodiesel was measured in terms of higher heating value (HHV) and was determined to be 40.44 MJ/kg, that is enough and considered as a good fuel characteristic for biodiesel.

Table 5.11: Physicochemical properties of *J. curcas* biodiesel and comparison with standards and reported biodiesel.

Properties	**Jatropha biodiesel (This study)**	**ASTM D6751**	**EN 14214**	**Reported biodiesel**								
				Honne seed oil (Olatundun et al., 2020)	***J. curcas* oil** (Chouhan and Sarma, 2013)	***J. curcas* oil** (Sarma et al., 2014)	**Yellow oleander-rubber oil** (Falowo and Betiku, 2022)	***J. curcas oil*** (Kumar et al., 2016)	***Moringa oleifera* oil** (Forouta n et al., 2022)	**Palm kernel oil** (Odude et al., 2019)	***Azadira chta indica* oil** (Etim et al., 2018)	**WCO** (Daimary et al., 2022b)
Density at 15 ^{o}C (g/cm^{3})	0.8757	0.86–0.90	0.86–0.90	0.870	0.891	0.875	0.887	0.875	0.874	-		0.88
Kinematic viscosity at 40 ^{o}C (mm^{2}/s)	4.027	1.9–6.0	3.5–5.0	5.98	6.8	5.7	-	4.75	4.1	4.7	5.0	3.90
Cetane number	50.3	47 (min)	51 (min)	55.1126	-	48.6	55	48.3	55.56	44.4		52
Cetane index	57.58	NS	NS		-	-	-		-	-		-
Pour point (^{o}C)	0	NS	NS		-	3	-	-6	-1	-3		-6

CFPP (^oC)	<4	NS	NS		-	-	-	-	-	-		-
SN (mg KOH/g)	191.28	NS	NS		-	-	-	-	-	-		-
Iodine value (g I_2/100 g)	76.70	NS	120 (max)	76.14	-	119	75.65	74.5	-	24.7	58.6	-
API	34.28	36.95	NS		0.892	0.875	-	-	-	30.51		-
Diesel index	66.08	50.4	NS		-	-	-	-	-	47.87		-
Aniline point	192.77	331	-		-	-	-	-	-	-		-
HHV (MJ/kg)	40.44	NS	NS	39.66	37.100	39.25	39.70	38.35	-	-	48.7	39.80

WCO–Waste cooking oil; NS–Not specified; max– maximum; min– minimum; CFPP–Cold filter plugging point; SN–Saponification number; API–American petroleum index; HHV–Higher heating value.

5.4 Conclusion

This study has successfully derived an efficient solid catalyst with high catalytic activity from the post-harvested waste of Bharatmoni for biodiesel production using *J. curcas* oil. The order of catalytic activity and biodiesel yield under the optimized conditions were found as CBS-550 (96.97 % in 12 min) > CBP-550 (96.89 % in 16 min) > CBR-550 (96.53 % in 18 min). This reactivity order follows the trends of the amount of potassium present in the catalysts which is in the sequence of CBS-550 (46.88 wt. %) > CBP-550 (44.88 wt. %) > CBR-550 (39.33 wt. %) from EDX analyses. The investigated pH value, basicity, and TOF values of CBS-550 are greater than CBP-550 and CBR-550 catalysts, which are also the reasons for achieving the higher activity. The FESEM, BET and HRTEM affirmed that the present calcined catalysts consist of porous materials which are primarily mesoporous. The reaction of the present work follows the kinetics model of pseudo-first order and demonstrated an endothermic process, which is endergonic and non-spontaneous. The CBS-550 catalyst (44.36 kJ mol^{-1}) showed a lower E_a value than CBP-550 (48.56 kJ mol^{-1}) and CBR-550 (49.26 kJ mol^{-1}) catalyst. The CBS-550 catalyst showed satisfactory reusability up to the 3rd cycle with 93.20 % product yield at optimized conditions. Therefore, the catalysts derived from the post-harvested Bharatmoni waste are attractive and significant for their catalytic characteristics. The preparation method of the catalyst is very simple, directly applicable in transesterification, and it is non-toxic, renewable, and low-cost catalyst possessing high catalytic activity for production of biodiesel."